Towards Estimation of Seasonal Water Dynamics of Winter Wheat from Ground-Based L-Band Radiometry

Thomas Jagdhuber[1,2], François Jonard[3,4], Anke Fluhrer[1,2], David Chaparro[5], Martin J. Baur[6], Thomas Meyer[4] and María Piles[7]

[1] German Aerospace Center, Microwaves and Radar Institute, Münchener Strasse 20, 82234 Wessling, Germany
[2] Institute of Geography, University of Augsburg, Alter Postweg 118, 86159 Augsburg, Germany
[3] Agrosphere (IBG-3), Institute of Bio- and Geosciences, Forschungszentrum Jülich GmbH, 52428 Jülich, Germany
[4] Earth and Life Institute, Université catholique de Louvain, 1348 Louvain-la-Neuve, Belgium
[5] Universitat Politècnica de Catalunya, CommSensLab & IEEC/UPC, Jordi Girona 1-3, 08034 Barcelona, Spain
[6] University of Cambridge, Department of Geography, Philippa Fawcett Dr, CB3 0AS, Cambridge, U.K.
[7] Image Processing Lab, Universitat de València, 46980 Valencia, Spain

Correspondence to: Thomas Jagdhuber (Thomas.Jagdhuber@dlr.de), Tel.: +49-8153-28-2329

Abstract. The vegetation optical depth (VOD) parameter contains information on plant water content and biomass, and can be estimated alongside soil moisture from currently operating satellite radiometer missions, such as SMOS (ESA) and SMAP (NASA). The estimation of water fluxes, such as plant water uptake (PWU) and transpiration rate (TR), from these Earth system parameters (VOD, soil moisture) requires assessing potential (suction tension) gradients of water and flow resistances in the soil, the vegetation and the atmosphere, yet it remains an elusive challenge especially on global scale. Here, we used a field-scale experiment to test mechanistic models for the estimation of seasonal water fluxes (PWU and TR) of a winter wheat stand including measurements of soil moisture, VOD, and relative air humidity (RH) under a controlled environment. We utilized microwave L-band observations from a tower-based radiometer to estimate VOD of a wheat stand during the 2017 growing season at the Selhausen laboratory in Germany. From VOD, we first extracted the gravimetric moisture of vegetation and then determined subsequently the relative water content (RWC) and the vegetation water potential (VWP) of the wheat field. Although the relative water content could directly be estimated from VOD, our results indicate this may be problematic for the phenological phases, when rapid biomass and plant structure development take place in the wheat canopy. The water uptake from the soil to the wheat plants was estimated from the difference between the soil and vegetation potentials divided by flow resistance from soil into wheat plants. The transpiration rate from the wheat plants into the atmosphere was obtained from the difference between the vegetation and atmosphere potentials divided by flow resistances from plants to the atmosphere. For this, the required soil matric potential (SMP), the vapor pressure deficit and the flow resistances were obtained from on-site observations of soil, plant and atmosphere and simple mechanistic models. This pathfinder study shows that the L-band microwave radiation

contains valuable information on vegetation water status that enables the estimation of water dynamics (up to

35   fluxes) from the soil via wheat plants into the atmosphere, when combined with additional information of soil and

atmosphere water content. Still, assumptions when estimating the vegetation water potential from relative water

content as well as when estimating the water flow resistances between soil, wheat plants and atmosphere had to be

made. Moreover, validation of water flux estimates for assessing their absolute accuracy could not be performed

due to a lack of in situ PWU and TR measurements. Nonetheless, our estimates of water status, potentials and

40   fluxes show the expected temporal dynamics and intercompare reasonably well in absolute terms, providing

confidence in further developing the proposed approach. Our findings support that passive microwave remote

sensing techniques allow for the estimation of vegetation water dynamics next to traditionally measured stand-

scale or plot-scale techniques. This might shed light on the potential capabilities of monitoring water dynamics in

the soil-plant-atmosphere system using wide-area, remote sensing-based Earth observation data.

45

1 Introduction

The monitoring of water dynamics between soil, vegetation and atmosphere and therefore the water availability

for plants asks for a system-driven and holistic approach integrating the three water storage compartments. The

Soil-Plant-Atmosphere System (SPAS) is such an approach linking the water, energy and carbon cycles (Reichardt

50   and Timm, 2014; Manzoni et al., 2013a; Ritchie, 1981; Cowan, 1965). It is understood as a physical continuum,

in which water dynamics occur as interdependent transfer processes between the three system compartments

(Nobel, 2020). Gardner (1960; 1965) was among the first to study the system holistically and to point out that the

water in the system flows in the direction of decreasing energy leading to the concept of water potential in soil,

plant and atmosphere (Gardner, 1960; Gardner, 1965; Slayter & Taylor, 1960). A gradient in water potential

55   induces a flow, for instance, from soil via roots and plant parts into the atmosphere decelerated by the resistance

of the traversed system compartments (Oosterhuis and Walker, 1987; Choudhury and Idso, 1985; Yan and Jong,

1971).

The water potential (WP) refers to the potential energy of water and is a key variable in plant physiology (Reichardt

and Timm, 2014). Since plants are the central component of the SPAS, the decreasing gradient in WP from soils

60   to the atmosphere drives the movement of water through plants (Elfving et al., 1972; Pearcy et al., 2012). Thus,

the vegetation water potential (VWP) changes according to the water availability in soils and the uptake capabilities

of the plant root and xylem systems, according to the regulation of transpiration through the stomata in leaves, and according to the vapor pressure deficit in the atmosphere (Lambers et al., 2008; Jonard et al., 2020).

65 The water transport through the different compartments of the SPAS is coordinated by adaption of potentials and resistances, in a way that water transport and water use efficiency are maximized by the plants, avoiding high-resistance conditions with plant-damaging water potential drops (Tyree and Zimmermann, 2013). According to Manzoni et al. (2014), the coordinated behavior is an outcome of plant adaption to their habitat by optimizing water use and gain in carbon assimilation for plant growth.

70 Under drought conditions, VWP changes due to a differing water transport through the plant, mainly regulated by stomata closure (Choat et al., 2018; Johnson et al., 2018). Hence, VWP is linked to the regulation of water transport and storage within plants (isohydric to anisohydric behavior) and thereby mechanistically relates key processes in the water, energy and carbon cycles (Lambers et al., 2008; Martinez-Vilalta and Garcia-Forner, 2017). In particular, estimating VWP from satellites would be interesting for regional and global ecological studies addressing drought impacts, especially on forest and agricultural ecosystems (e.g. Feldman et al., 2020). Such

75 retrievals would also be highly applicable to inform global vegetation, Earth system, or atmospheric boundary layer models (Bonan et al., 2014; Matheny et al., 2017; Moment et al., 2017; Momen and Bou-Zeid, 2017).

Microwave remote sensing retrieval approaches up to satellite observation missions (e.g. SMOS (ESA) or SMAP (NASA)) often deal with estimating the status of Earth system parameters (like soil moisture) rather than with assessment of dynamic flow processes, like water uptake or transpiration of plants (Entekhabi et al., 2010; Kerr et

80 al., 2010; Portal et al., 2020). An exception in terms of estimation of water dynamics is the GRACE mission (Sadeghi et al., 2020a), assessing total water storage change, and especially its combination with the SMOS and SMAP missions (Sadeghi et al., 2020b). The estimation of water dynamics from remote sensing requires assessing potential (suction tension) gradients of water rather than (storage) filling status of soils or plants with water.

Passive microwave remote sensing techniques should be capable to obtain VWP-estimates, provided that plant

85 hydraulic trait information is available (Konings et al., 2019). To do so, the vegetation optical depth (VOD) parameter that measures the degree of attenuation of microwaves as they pass through vegetation needs to be first extracted from the radiometer observations by model-based parameter retrievals. Afterwards the biomass and water contributions to the VOD parameter need to be disentangled (Martinez-Vilalta et al., 2019). As proposed in Bonan et al. (2014), the relative water content (RWC) can be a valid metric for plant water status and can be utilized to

90 estimate VWP. Konings et al. (2019) explained how microwave remote sensing can be applied for monitoring of plant parameters, like RWC. In addition, Rao et al. (2019) showed that VOD from X-band satellite radiometry can

be converted into RWC-estimates with the caveat that both, water and biomass, influence the VOD especially in seasonally growing agricultural species, like winter wheat. Therefore, only periods with constant biomass should be evaluated in order to isolate the water component directly from VOD. Fink et al. (2018) found a way to extract

95   the gravimetric moisture of vegetation (m_g) from the VOD-signal. m_g can be converted into RWC and, importantly, it is not affected by biomass dynamics. The m_g-estimation methodology of Fink et al. (2018) was further developed and validated at the field-scale in Meyer et al. (2019).

For the present study, the dataset of Meyer et al. (2019) is used to estimate water potential and water flux along SPAS for the 2017 growing season of a winter wheat field. The winter wheat field was monitored with the ground-

100   based L-band radiometer instrument ELBARA-II. Simultaneously, in situ measurements for key plant (e.g. m_g, height, biomass, leaf area index (LAI), and phenology), soil (e.g. relative permittivity and moisture) and atmosphere (e.g. air temperature, wind speed, net radiation and relative humidity) properties were recorded directly within the test field.

The objective of this study is to research the feasibility to estimate potentials and seasonal flux rates of water (water

105   uptake from soil and transpiration rates into the atmosphere) within the SPAS of a winter wheat field starting from ground-based L-band radiometry in combination with on-site measurements of soil and atmosphere. Our research question is whether the combination of L-band radiometry and a confined set of on-site measurements are sufficient to arrive at reasonable water potential dynamics and water flux rates in the SPAS of a winter wheat field.

2 Test site and experimental data

110   The research study was carried out at the Selhausen remote sensing field laboratory, Germany (Jonard et al., 2015; Jonard et al., 2018). The experimental setup, considered in this study, consists of a 12 [m] x 20 [m] plot covered by a mesh reflector (metal grid) on the ground with winter wheat (*Triticum aestivum* L.) plants growing through it. L-band (1.4 [GHz]) passive microwave measurements were performed using an ELBARA-II radiometer of Forschungszentrum Jülich (FZJ) fixed at 4 [m] height. ELBARA-II features a dual-mode conical horn antenna with

115   an absolute accuracy of 1 [$°K$] and relative sensitivity of < 0.1 [$°K$] (Meyer et al., 2018). Radiometer measurements were repeated twice a week at incidence angles between 40° and 60° in 5° increments.

Solely the vegetation microwave radiation is measured using a mesh reflector on the ground and the radiation from the soil is blocked by the reflector (Jonard et al., 2015). In situ measurements of soil texture (silt loam with 13 [$\%$] sand, 70 [$\%$] silt, and 17 [$\%$] clay), soil permittivity and soil temperature were obtained every 15 [min] (and every

120   30 [min]) using 15 capacitance sensors installed at 5 [cm] (and using 30 time-domain reflectometry (TDR) sensors

installed at 30 [cm]) depth in direct vicinity of the radiometer footprint within the field. Soil permittivity measurements can be converted to soil moisture θ according to the well-established dielectric mixing model of Topp et al., (1980). Precipitation, net solar radiation, air temperature, wind speed and relative humidity data come in 10 [min]-resolution (except for wind speed at 30 [min]-resolution) from the TERENO climate station located

125   next to the field laboratory. In order to be less dependent on in situ measurements, also L-band radiometer-derived soil moisture data could have been used from a non-meshed area of the winter wheat field instead of the in situ soil permittivity measurements. However, the in situ data have a significantly higher temporal resolution than the radiometer observations. But similar to the soil permittivity, also these data could be derived from remote sensing-based approaches in a future, more in situ-independent, larger-scale research study.

130   Vegetation height [m], leaf area index (LAI) [$m²/m²$], above ground biomass (AGB) [$kg/m²$], and vegetation water content (VWC) [$kg/m²$] were measured destructively every week around the radiometer measurements for comparison and validation. All vegetation-related measurements of the growing season in 2017 and the different phenological phases are presented in Figure 1 and Table 1. For a detailed description of the trends and dynamics of these on-site measurements as well as a full sketch of the experimental setup, the reader is referred to Meyer et

135   al. (2018) and Meyer et al. (2019).

Table 1: Overview of growth stages of the winter wheat between 10th of April (DOY 100) and 14th of August 2017 (DOY 226) and their corresponding phenological phase (after BBCH (Biologische Bundesanstalt, Bundessortenamt und CHemische Industrie) code) (Meyer et al., 2018).

DOY 2017	Growing stage	BBCH code
100	Tillering	26
108 - 122	Stable stem elongation	30
128 - 142	Further stem elongation (increased plant growth rate)	35
142 - 149	50 % of inflorescence visible	55
157	Beginning of flowering	61
163	Grain development started	71
180	Grain fully developed and start of ripening process	77 and 83 - 89
190 - 226	Early senescence until late senescence	92 -99
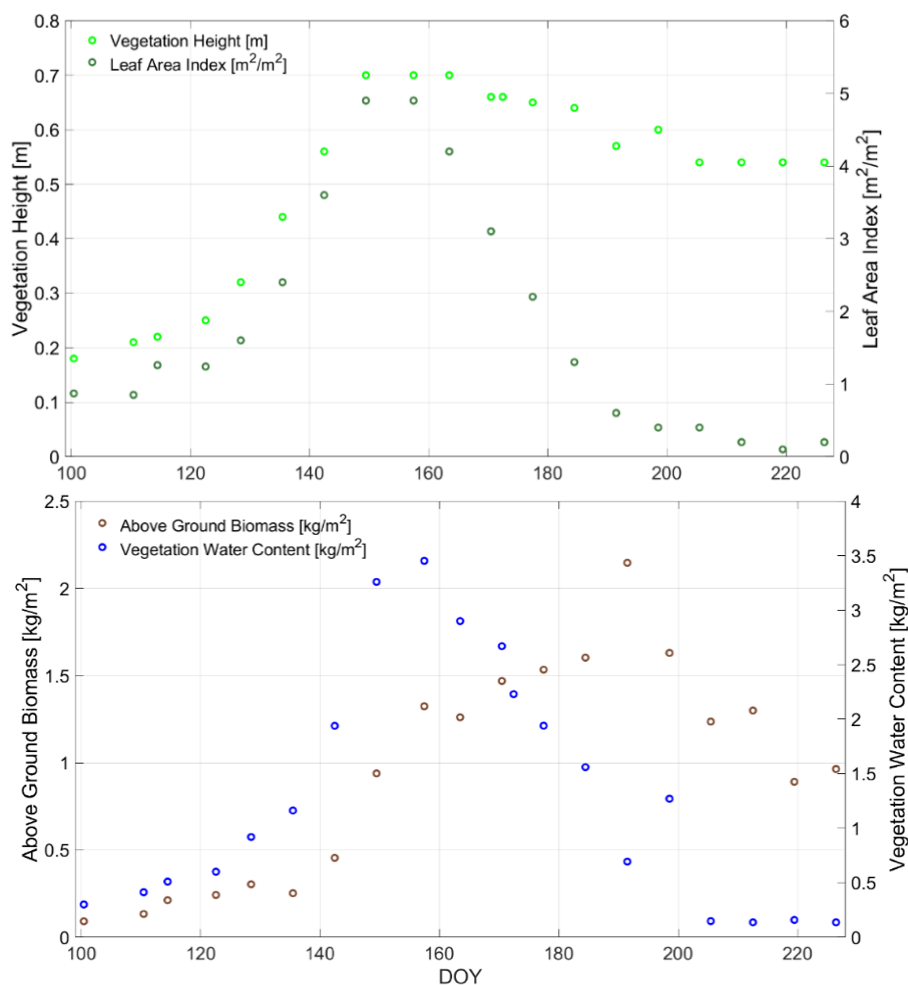
Figure 1: In situ measurements of the wheat field along growing season for days of year (DOY) in 2017 at the Selhausen field laboratory, Germany: Vegetation height [m] & leaf area index (LAI) [$m²/m²$] (top); above ground biomass (AGB) [$kg/m²$] & vegetation water content (VWC) [$kg/m²$] (bottom) (Meyer et al., 2018).

3 Methodology of water dynamics estimation

The methodology for water dynamics estimation - water uptake from soil to wheat vegetation (PWU) & transpiration from wheat vegetation to atmosphere (TR) - is conceptualized in the workflow of Figure 2. First, the water status of soil (θ), vegetation (m_g; cf. section 2) and atmosphere (RH) need to be known from remote sensing estimates or on-site measurements. From the status, the water potentials for the three environmental compartments (soil, vegetation & atmosphere) are calculated (sections 3.1 to 3.3) and then SMP and VWP are used to retrieve the water uptake from the soil into the wheat vegetation (section 3.4). In addition, the atmospheric water potential,

150   usually expressed by the vapor pressure deficit (VPD), is applied together with the VWP to calculate the

transpiration rate of the wheat vegetation into the atmosphere (section 3.5).
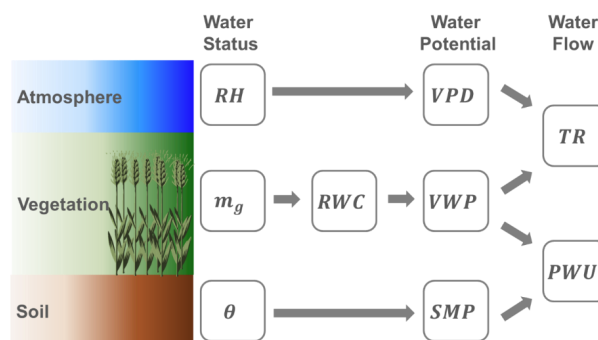
Figure 2: Processing workflow for estimation of soil, vegetation and atmosphere water potentials (SMP= Soil Matric Potential, VWP = Vegetation Water Potential, VPD = Vapor Pressure Deficit) and water fluxes (PWU = Plant Water

155   **Uptake, TR = Transpiration Rate) from storage variables (θ = Soil Moisture, m_g = Vegetation Water Content (gravimetric), RH = Relative Air Humidity).**

3.1 Soil Matric Potential (SMP) from Soil Moisture (θ)

The fundamental force describing the overall state and movement of water within the soil is energy: kinetic or

160   potential (Hillel, 1980). The kinetic energy is assumed to be negligible in agricultural (wheat-covered) soils due to

the overall slow movement of soil water in fields with no to moderate slopes (Hillel, 1980; Shukla, 2014). The

potential energy, however, is important when describing the movement of water in soils and the water retention

forces against percolation towards ground water level. Hence, the rate of decrease in potential energy with distance

is actually the driving force which causes water to flow within soils (Hillel, 1980). The difference in energy states

165   between the soil water and pure free water (i.e. reference potential) is defined as total soil water potential. In

unsaturated soils various forces, such as capillary or adsorption, act on soil water, which causes soil water potential

to be less than that of pure water in reference conditions (known as suction tension).

Due to the different forces influencing the soil water, the total soil water potential is mainly the sum of pressure,

gravitational and osmotic potentials (Hillel, 1980; Shukla, 2014). Since the pressure potential is defined as the

170   water potential resulting from capillary and adsorptive forces acting on the soil matrix, it is generally called the

SMP or matric suction (Hillel, 1980; Shukla, 2014); it can be expressed in energy per unit mass [J/kg], in energy

per unit volume (pressure: [bar] or [Pa]), or energy per unit weight (hydraulic head: [cm] or [pF]) (Hillel, 1980;

Shukla, 2014, Ward and Robinson, 2014).

The SMP is dependent on θ and vice versa. The relationship between both parameters is described by the soil

175   water retention curve. Water retention subsumes all mechanisms and processes related to changes soil moisture

and its energy state (Gupta and Wang, 2006). The shape of the soil water retention curve is dependent upon various soil characteristics (e.g., texture, and particularly clay fraction), as well as on the current and previous states of θ (Hillel, 1980; Ward and Robinson, 2014).

When investigating plant growth, two common values of SMP are of major interest: the permanent wilting point

180 and the field capacity. The wilting point (around SMP of -1.5 [MPa]) is defined as the minimum soil water content at which most crop plants can still extract water from the soil (Nobel, 2020, p. 542). The field capacity, reported for instance at -0.01 [MPa] in Ward and Robinson (2014) or at -0.033 [MPa] in Gupta and Wang (2006), corresponds to the amount of remaining water after a saturated soil drained under gravity for one to two days following a precipitation event. Exact values for each soil are dependent on the individual soil characteristics. The

185 difference between field capacity and wilting point is regarded as available water that can be taken up by plants (Ward and Robinson, 2014; Gupta and Wang, 2006). Besides tensiometer or thermocouple psychrometer, which can directly measure SMP (Hillel, 1980; Gupta and Wang, 2006), several soil water retention models exist to estimate SMP from θ. The most widely used ones are from Brooks & Corey (Brooks and Corey, 1964), Campbell (Campbell, 1974), or Van Genuchten (van Genuchten, 1980). In this study we apply the Campbell model to

190 estimate SMP from θ measurements:

$$SMP = \left(SMP_s \ast \left(\frac{\theta}{n} \right)^{-b} \right), \tag{1}$$

with SMP_s as matric potential at field capacity (saturated suction), n representing soil porosity, and b as empirically determined constant characterizing the pore-size distribution of the soil (Margulis, 2017; Campbell,

195 1974). The values for SMP_s and b for (1) are provided by Clapp & Hornberger, where representative values for hydraulic parameters are presented for various soil textures (Clapp and Hornberger, 1978). The values for the soil type silty loam at Selhausen are SMP_s = -0.786 [m], $n = \theta_s \cdot f_s$ (including soil moisture content at field capacity θ_s = 0.485 [-] from Clapp & Hornberger and silt fraction from soil surveys at the test site f_s=0.7 [-]) and b = 5.3 [-] (Clapp and Hornberger, 1978). Values for θ originate from *in situ* relative permittivity measurements from 5 [cm]

200 and 30 [cm] soil depth (cf. section 2).

3.2 Relative Water Content (RWC) and Vegetation Water Potential (VWP) from Vegetation Moisture (m_g)

The m_g of the winter wheat field [kg/kg] was firstly estimated in Meyer et al., 2019 from ground-based L-band radiometer data, acquired between 9 am and 2 pm at 40° incidence angle. In this process, the VOD was retrieved via radiative transfer model inversion from the V-polarized brightness temperature measurements of ELBARA-

205 II. Afterwards m_g was estimated from VOD by inversion of the forward model proposed by Schmugge & Jackson (Meyer et al., 2019; Schmugge and Jackson, 1992; Ulaby and El-Rayes, 1987). Full details are provided in Meyer et al., 2019.

m_g is a metric of kilogram water per kilogram wet biomass and can be converted into a change metric, called relative water content RWC [%] by putting boundaries on upmost (maximum $m_{g_{max}}$) and lowest (minimum

210 $m_{g_{min}}$) m_g (Pearcy et al., 2012; Easmus et al., 2016; Smart and Bingham, 1974):

$$RWC = \frac{m_g - m_{g_{min}}}{m_{g_{max}} - m_{g_{min}}} \cdot 100, \tag{2}$$

As these boundary conditions are found for this study along the measured growing season in 2017 within the winter wheat field, the RWC serves here as a relative metric referring to the water dynamics of the recorded season

215 (RWC_{Season}). Since m_g-estimates are obtained only once at a measuring day, it limits the chance to capture the true minimum and maximum of the 2017 growing season. However, the $m_{g_{min}}$ is found in the senescence phase where the water content drops to a minimum (see low and constant level of VWC in Figure 1 for the senescence phase). More challenging is the detection of the maximum $m_{g_{max}}$ of the season due to the temporally sparse measurements, therefore using in the end the maximum of the m_g-timeseries as $m_{g_{max}}$. Note RWC_{Season} by

220 definition is not representative for water dynamics on shorter time scales than seasons, like at weekly or even diurnal scales or for single phenological phases (Passioura, 1982).

For the next step, Zweifel et al. in 2000 and 2001 described a semi-empirical model linking the RWC [%] to its VWP [MPa] (Zweifel and Häsler, 2000; Zweifel et al., 2001):

$$VWP = \frac{VWP_{min}}{e^{\frac{-k_1 + RWC}{k_2}} + 1}, \tag{3}$$

225 where k_1 and k_2 are empirical parameters representing the inflection point of the function, and the rate of change between RWC and VWP, respectively. VWP_{min} [MPa] is the minimum of VWP assumed for the relationship. All three parameters are plant type specific and need plant-specific adaption, since the parameterization of Zweifel et al. was done for trees (Zweifel and Häsler, 2000; Zweifel et al., 2001). In this study we adapt the parameterization for winter wheat with VWP_{min} of -2.5 [MPa] (Frank et al., 1973; Gupta et al., 1989; Kameli and Lösel, 1993;

230 Rascio et al., 1994, Siddique et al., 2000). Figure 3 illustrates the RWC-VWP relationship for slow (k_1=55;

k_2=10), intermediate (k_1=68; k_2=7.5) and rapid (k_1=81; k_2=5) change dynamics according to literature studies (Turner and Long, 1980; Turner, 1988; Zweifel et al., 2001; Pearcy et al., 2012; Konings et al., 2019). The sigmoidal dynamics in Figure 3 should cover the potential variation of dynamics for wheat, as understood from literature, but with no means of being exhaustive or fully precise.
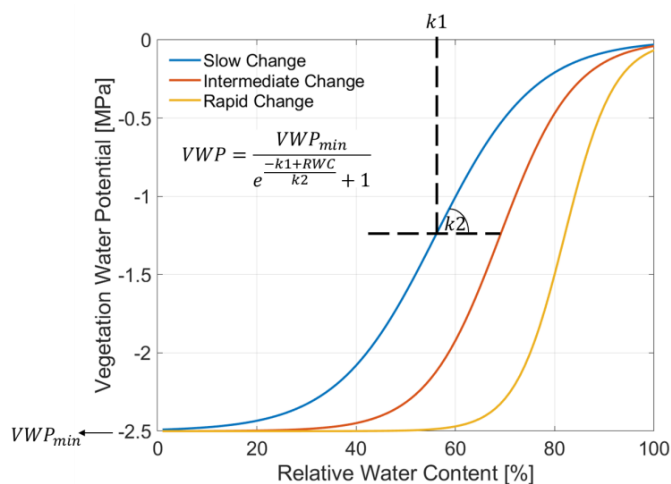
Figure 3: Modelled relation between Relative Water Content (RWC) [%] and Vegetation Water Potential (VWP) [MPa] adapted for winter wheat and assuming different rates from slow (blue color) to intermediate (red color) until rapid (orange color) change. The inset equation, adopted from Zweifel and Häsler (2000) and Zweifel et al. (2001), integrates a minimum VWP (VWP_{min}) and specifies an inflection point (k_1) and a rate (k_2) of the change dynamic between RWC and VWP. k_1 and k_2 are also indicated schematically with dashed black lines.

3.3 Atmosphere Water Potential (Vapor Pressure Deficit - VPD) from Relative Humidity (RH) and Air Temperature (T_{Air})

In unsaturated air conditions the atmosphere shows a deficit of water vapor indicating the water potential of the atmosphere. Atmospheric vapor pressure deficit (VPD) is defined as the difference between the actual water vapor pressure and the saturation water vapor pressure at a particular temperature. It can be calculated as follows (Reichardt and Timm, 2014; Castellvi et al., 1996):

$$VPD = P_{sa}(1 - RH), \qquad (4)$$

Including the relative humidity of the air RH [-] and saturation water vapor pressure of the air $P_{sa} = 0.61094 \cdot \exp(17.625 \cdot T_{Air}/(T_{Air} + 243.04))$ [kPa], where T_{Air} represents the air temperature [$°C$] (Alduchov and Eskridge, 1996). In this study RH and T_{Air} are measured at 2 [m] height above ground at the on-site

meteorological station. Time series of VPD and its input variables (RH, T_{Air}) for the period of study are presented in Figure 4.

255
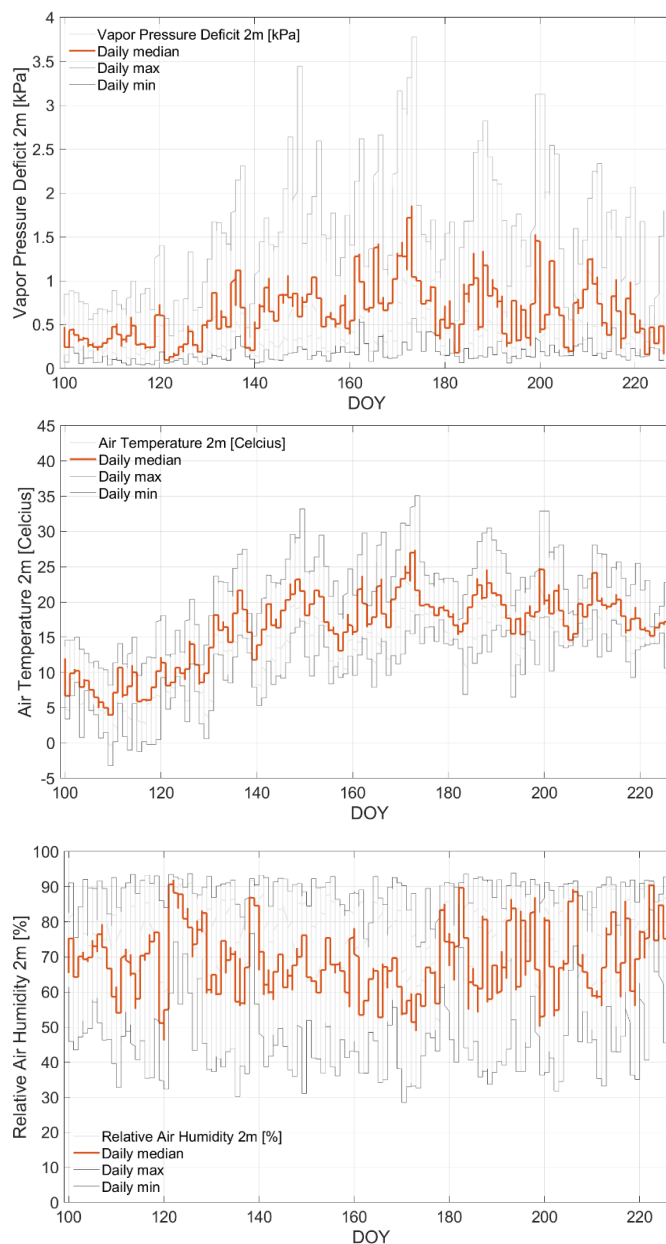
Figure 4: Calculated Vapor Pressure Deficit (VPD [kPa]) at 2 [m] height (top plot) from measurements of air temperature ([T [°K]) (middle plot) and relative humidity (RH [%]) (bottom plot) using Equation (4) in the growing
260 **period of 2017 along days of year (DOY) in 2017 at the winter wheat field in Selhausen, Germany. Colored and gray curves indicate daily median, minimum and maximum of measurements and estimates.**

3.4 Water Uptake (PWU) from Soil into the Wheat Plants

The water uptake process follows from hydraulic potential gradients and flow resistances in the SPAS. The principle of potential difference by flow resistance is motivated from the field of electricity by Ohm's law. Van
265   den Honert in 1948 was one of the first realizing and showing this connecting concept (Van den Honert, 1948; Cowan, 1965, Monteith and Unsworth, 2013; Nobel, 2020).

The PWU [mm/s] from the soil into the winter wheat plant can be defined as the potential difference (converted to [mm]) between the soil (SMP) and the vegetation (VWP) divided by the resistance (e.g. in the rhizosphere, roots and xylem along SPAS (Van den Honert, 1948; Wallace, 1978; Wallace and Biscoe, 1983)):

270

$$PWU = \frac{SMP - VWP}{R_{RX} + R_S},$$ (5)

where R_{RX} [s] is the resistance against water flow in roots and xylem of the wheat plants (Lynn & Carson, 1990) and R_S [s] is the resistance for water uptake from the soil into the wheat roots. Since R_S and R_{RX} cannot be measured in situ at field scale along the growing season (Wallace, 1978; Wallace and Biscoe, 1983; Ruggiero et al.,
275   2007), all resistances in this study are effective values with no claim on absolute accuracy.

We adopt the approach of Feddes and Rijtema (1972) estimating the R_S from soil hydraulic conductivity [m/s], based on the Campbell model (Campbell, 1974; Choudhury and Idso, 1985; Lynn and Carlson, 1990; Dingman, 2015; Meyer et al., 2018). We use soil moisture [m^3/m^3] (converted from soil permittivity) and soil parameters for silty loam from Clapp & Hornberger (1978) and Steenpass et al. (2010), and a rooting depth of one meter according
280   to literature (Fan et al., 2016). Figure 5 shows estimates of soil resistance [s] from Feddes and Rijtema (1972) based on soil hydraulic conductivity [m/s] at 5 [cm] and 30 [cm] soil depth.
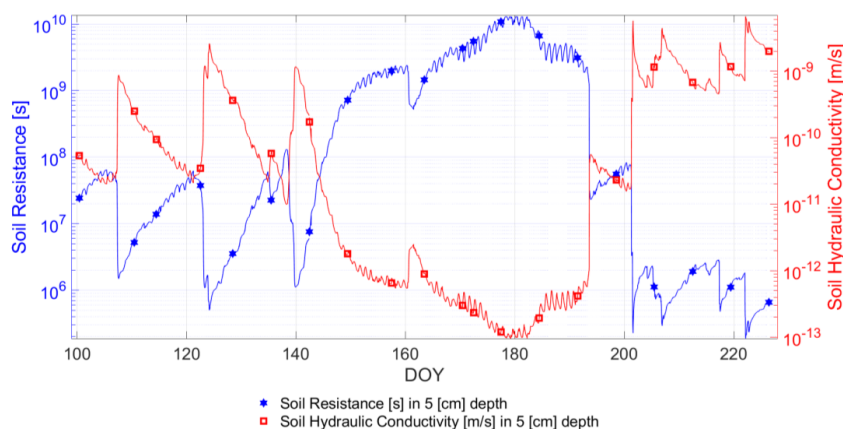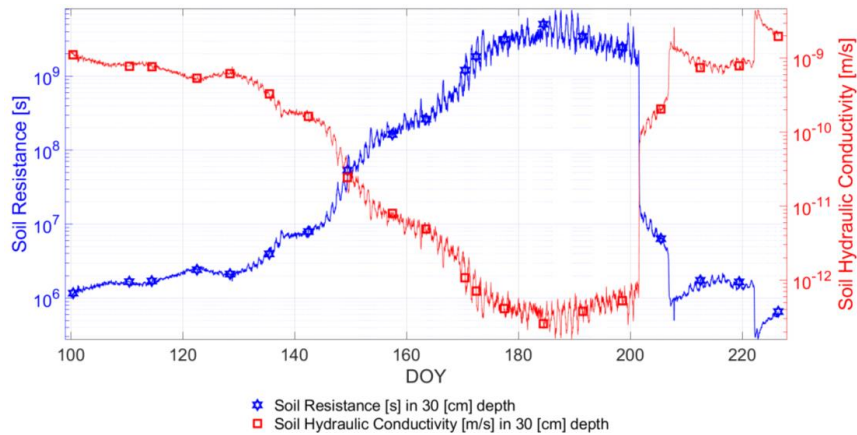
285 **Figure 5: Comparison of the soil permittivity-derived and Campbell (1974) model-based soil hydraulic conductivity**
$[m/s]$ **and the calculated soil resistance** R_S $[s]$ **from the model of Feddes and Rijtema (1972) implemented according**
to Choudhury and Idso (1985): at 5 $[cm]$ **(top) and 30** $[cm]$ **(bottom) soil depth; symbols indicate radiometer observation**
dates along days of year (DOY).

290

For the root-xylem resistance R_{RX} we deduced a LAI-based linear model from an approach combining in situ

measurements with boundary layer modelling, detailed in Lynn and Carlson (1990, Fig. 16):

$$R_{RX} = (-LAI \cdot 0.007 + 0.05) * C_U, \qquad (6)$$

295

where LAI $[m^2/m^2]$ is measured in situ (cf. Fig. 1) and $C_U = 0.4 \cdot 10^{10}$ represents the unit conversion from

$[bar\,(W/m^2)^{-1}]$ to $[s]$. Figure 6 shows R_{RX} along the growing period and its linear relation to LAI.
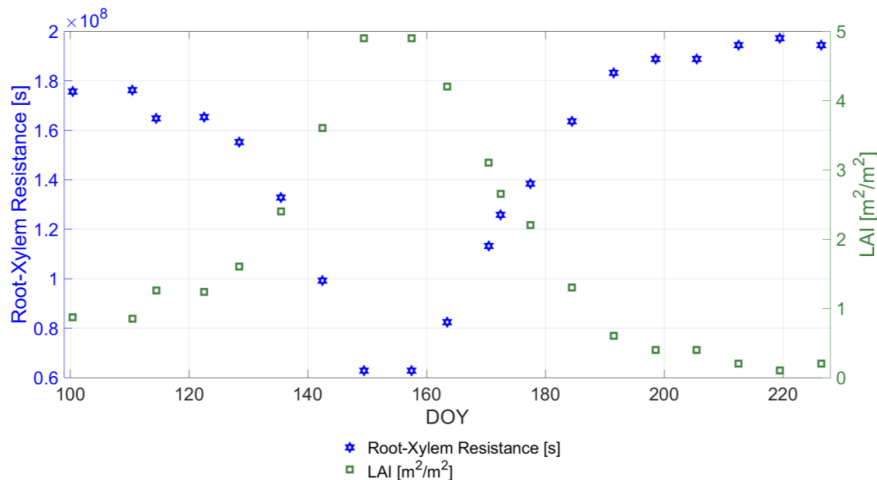
Figure 6: Comparison of the in situ-measured leaf are index LAI $[m^2/m^2]$ **and the calculated root-xylem resistance**
300 R_{RX} $[s]$ **deduced from Lynn & Carlson (1990) along days of year (DOY).**

3.5 Transpiration (TR) from Wheat Plants into Atmosphere

The wheat transpiration rate TR [mm/s] from the wheat plants into the surface-proximate is expressed as the

potential difference between the vegetation (VWP) and the atmosphere (VPD) (at 2 [m] height above ground)

divided by the resistance of the upper (adaxial) and lower (abaxial) side of the leaves and their respective stomata

305   against water vapor outgassing and the resistance of the surrounding atmosphere (Reichardt and Timm, 2014,

p.277ff; Pearcy et al., 2012, p175ff; Nobel, 2020, p.415ff):

$$TR = \frac{VPD - VWP}{R_A + 2R_C + 2R_{ST}}, \tag{7}$$

where R_A [s/m] is the aerodynamic resistance of the proximate atmosphere to absorb the vaporized moisture

310   (Allen et al., 1998; Monteith, 1965; Chouhury and Idso, 1985). R_C [s/m] is the cuticular resistance of the leaf

surface for direct transpiration through epidermis (fixed to $R_C = 4 \cdot 10^3$ [s/m]) (Monteith and Unsworth, 2013;

Nobel, 2020, p.415). R_C is of minor influence in this study due to non-drought conditions (Duursma et al., 2019).

It is included for simplicity as an additive resistance component in (7) (Nobel, 2020, p.427ff). R_{ST} [s/m] is the

resistance of the wheat canopy stomata against transpiration (Gallardo et al., 1996). Damour et al. in 2010 provide

315   a comprehensive overview of stomatal resistance models. Choudhury and Idso (1985) proposed an empirical model

for canopy stomatal resistance of field-grown wheat stomata. It is adopted in the following to provide estimates of

time-varying stomatal resistance [$MPa\,s/m$] values for the winter wheat field (Choudhury and Idso, 1985), where

density of liquid water (997 [kg/m^3]) and latent heat of water vaporization ($2.2564 \cdot 10^6$ [J/kg]) are used to convert

units from [s/m] to [$MPa\,s/m$] to match the calculus in (7) (Monteith & Unsworth, 2013). On-site

320   measurements of solar net radiation [W/m^2] (cf. Fig. 1) and VWP were used as inputs to the model. The net radiation

as well as the stomatal resistance R_{ST}-values are displayed in Figure 7 and compare to values reported in Nobel

(2020, p. 421). Details of the implementation are provided in Choudhury and Idso (1985).

The aerodynamic resistance R_A is shown in Figure 8 and is a function of the wind speed (measured at 2 [m] height)

and the vegetation height (cf. Fig. 1). The R_A-calculus is adopted from Monteith,1963 and is also presented in Allen

325   et al., 1998 and Choudhury and Idso, 1985. Both resistance values (R_{ST}, R_A) are used together with R_C in (7) to

calculate time-dynamic transpiration rates TR.
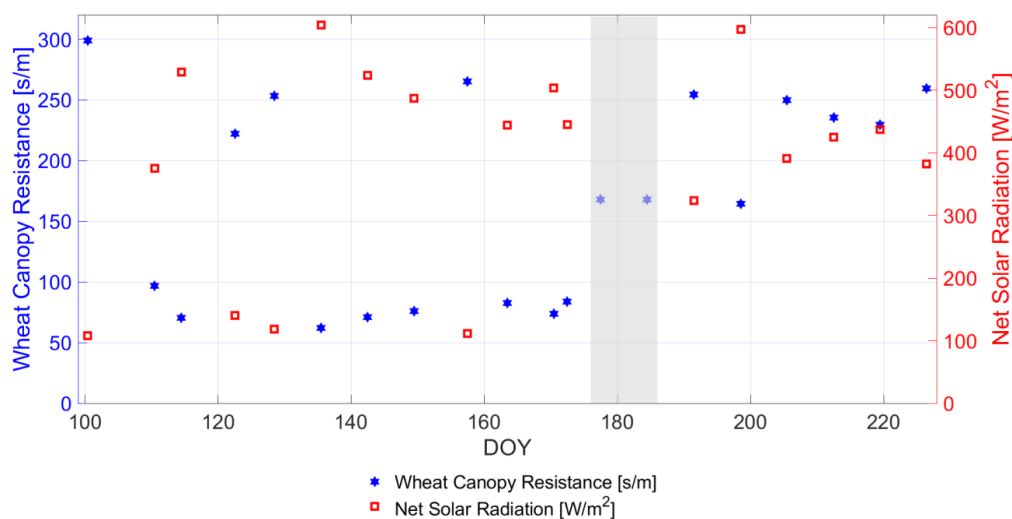
Figure 7: Comparison of the in situ measured net solar radiation $[W/m^2]$ and the calculated stomata resistance R_{ST} 330 $[s/m]$ of the winter wheat canopy from the model of Choudhury and Idso, 1985 under incorporation of VWP-observations (cf. Figure 1) along days of year (DOY); The gray area indicates two dates where no net solar radiation measurement were available and the resistance values for the canopy are set to fixed values of 168 $[s/m]$.
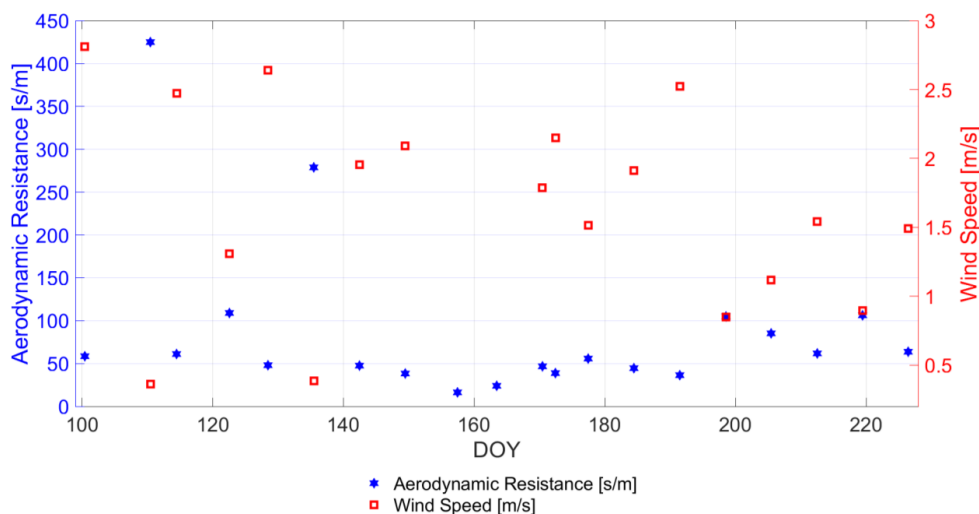
335 **Figure 8: Comparison of the in situ measured wind speed $[m/s]$ and the calculated aerodynamic resistance R_A $[s/m]$ of the winter wheat canopy from the model of Monteith, 1963 (adopted in Choudhury and Idso, 1985) under incorporation of vegetation height observations (cf. Figure 1) along days of year (DOY).**

340 Since R_A, R_C and R_{ST} are effective values (Wallace, 1978; Wallace and Biscoe, 1983) and not directly measurable

in situ for an entire wheat field (Selhausen test site) along the entire growing period (April to August 2017)

(Ruggiero et al., 2007; Blizzard and Boyer, 1980), they were retrieved in a model-based way as introduced above.

Table 2 provides a summary on the non-measured variables for estimation of plant water dynamics that were obtained from parameterizations and models in this study.

345 **Table 2: Summary of parameterizations and models for the non-directly measured variables in the estimation of plant water dynamics of winter wheat.**

Variable	Parameterization	Model / Reference
Soil		
Soil Matric Potential (SMP) [MPa]	Soil moisture, soil porosity n, soil texture (sand, silt & clay fractions) & pore size distribution b	Campbell, 1974; Clapp and Hornberger, 1978
Vegetation		
Relative Water Content (RWC) [%]	Gravimetric water content of winter wheat m_g	Pearcy et al., 2012; Smart and Bingham, 1974
Vegetation Water Potential (VWP) [MPa]	RWC & empirical calibration parameters (k_1, k_2)	Zweifel and Häsler, 2000; Zweifel et al., 2001
Plant Water Uptake (PWU) [mm/s]	VWP, R_S, R_{RX} & SMP	Monteith & Unsworth, 2013; Wallace, 1978; Van den Honert, 1948
Soil Resistance (R_S) [s/m]	Soil moisture, soil texture & rooting depth	Feddes and Rijtema, 1972; Campbell, 1974; Clapp and Hornberger, 1978
Root-Xylem Resistance (R_{RX}) [s/m]	LAI	Lynn & Carlson, 1990
Transpiration Rate (TR) [mm/s]	VWP, R_C, R_{ST}, R_A, & VPD	Reichardt and Timm, 2014, p.277ff; Pearcy et al., 2012, p.175ff; Monteith & Unsworth, 2013, p.191
Stomatal Resistance (R_{ST}) [s/m]	Solar net radiation & VWP	Choudhury and Idso, 1985
Aerodynamic Resistance (R_A) [s/m]	Wind speed & vegetation height	Allen et al., 1998; Choudhury & Idso, 1985, Monteith, 1965
Atmosphere		
Vapor Pressure Deficit (VPD) [kPa]	Relative air humidity & P_{sa}	Castellvi et al., 1996;
Saturation Water Vapor Pressure (P_{sa}) [kPa]	Air temperature	Alduchov and Eskridge, 1996

4 Results

The results are presented following the SPAS from soil to atmosphere starting with the water status in the soil,

350 continued by the water status in the wheat plants, moving on to the water dynamics from soil, via wheat plants into the surface-proximate atmosphere.

4.1 Water Status in the Soils

In Figure 9, the estimated SMPs at 5 [cm] and 30 [cm] soil depth are shown together with the soil permittivity of the top soil (5 [cm] below surface) and in the root zone (30 [cm] below surface) and the daily sum of precipitation.

355   It can be seen that *in situ* measured soil permittivity varies with precipitation impulse, increasing shortly after rain events. The soil in the root zone follows the dynamics of the top soil, but with a lower magnitude and on a broader time span.

For top soil, highest permittivity values are reached after the early senescence with ~15.5 [-], corresponding to a soil moisture value of ~28.4 [$vol.\%$]. From DOY 160 to DOY 190 the soil permittivity is constantly at a low level

360   of ~9 [-] (~16.8 [$vol.\%$]), since during that period almost no precipitation occurred. The high correlation between the SMP and soil permittivity curves at 5 [cm] as well as at 30 [cm] soil depth is a result of, on the one hand, the fact that soil permittivity is one of the main input parameters within the Campbell model to determine SMP, and, on the other hand, due to the water retention characteristics between θ and SMP (cf. section 3). After every rain event when soil permittivity is increasing, the SMP also increases towards less negative values. This is more

365   pronounced for the top soil layer than for the deeper one.

As the empirically fitted parameter b in (1) was set to 5.3, the obtained soil water retention curve is non-linear. This effect is visible during the dry period between DOYs 140 to 190, where the SMP is constantly decreasing to more and more negative values until DOY 180 and then constantly increasing towards less negative values again. While the soil permittivity is decreasing, the SMP is getting larger in magnitude, hence more negative in value. For

370   SMP at 30 [cm] soil depth, the drying period starts at DOY 150, meaning slightly delayed compared to SMP at 5 [cm] soil depth, as indicated in Fig. 9. The drying period affects the deeper soil layers longer (until DOY 200). Furthermore, at around DOY 185 the maximum suction tension with -0.15 [MPa] at around DOY 185 is lower (by 0.05 [MPa]) for soil in the root zone than for SMP in the top soil.

If SMP at -0.033 [MPa] is considered as field capacity, the estimated results are always indicating enough available

375   water for plants to be extracted from the soil across the entire period of investigation. However, if one considers the SMP at -0.01 [MPa] as field capacity, the winter wheat may have less available water some times during the stem elongation and after the early senescence phases. However rooting depth was not measured along the growing season of 2017, but would inform about the respective water reservoirs assessible for the wheat plants during the different phenological phases. During the period between DOY 178 and DOY 182 the results for SMP at 5 [cm]

380   depth show the highest suction tensions with values down to -0.2 [MPa], whereas the permanent wilting point is

around -1.5 [*MPa*]. This indicates a drier period for the wheat plants, although water from the soil was available for

the plants at any time during the season (cf. section 3).
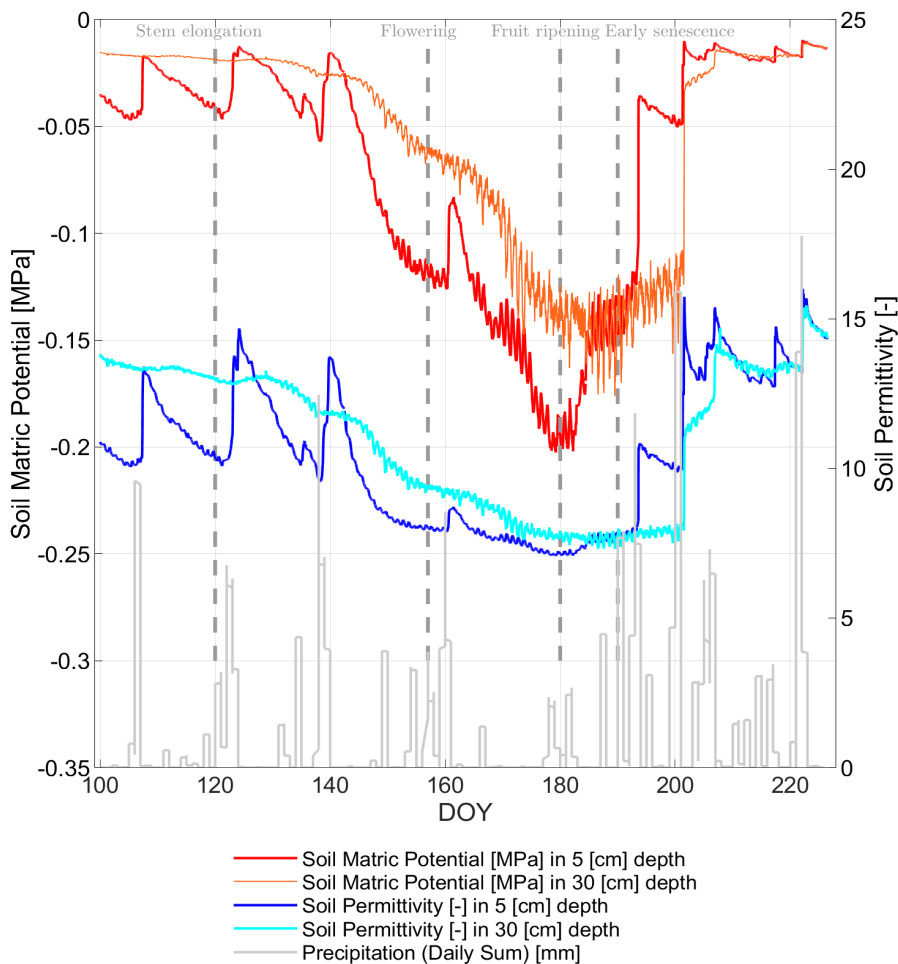
Figure 9: Comparison of the temporal evolution of Soil Matric Potential (*SMP*) [*MPa*], calculated after Campbell, 1974
385 **& Clapp and Hornberger, 1978 in 5 [*cm*] (red curve) and 30 [*cm*] (orange curve) soil depth from in situ measured soil**
permittivity [-] in 5 [*cm*] (blue curve) and 30 [*cm*] (cyan curve) along growing season of 2017 in days of year (DOY).
Gray bars indicate the daily sum of precipitation [*mm*] at the winter wheat field in Selhausen, Germany.

4.2. Water Status in Wheat Plants

390 For understanding the vegetation status along growing season, m_g [*kg/kg*] of the winter wheat is calculated

according to Meyer et al. (2019) and presented in Figure 10. We assumed vertical stalks as mainly affecting plant

component of winter wheat for L-band emission and within m_g-calculus for subsequent analysis in this study.

Figure 10 indicates the in situ measurements (gray crosses) and the radiometer-based estimates (blue circles) of m_g

along the wheat growing period (senescence from DOY 191). The overall dry down of the winter wheat along
395   growing season accompanied by the ripening of the plants until senescence is tracked by in situ measurements as
well as by the radiometer-based m_g-estimates.

However, it is apparent that the estimates arrive at a higher m_g-level in the senescence phase than the in situ
measurements (cf. Fig. 10, DOY 200-226), which can be explained by assuming in the retrieval of Meyer et al.
(2019) that the vegetation volume fraction stays constant along the growing season. This is a strong, but
400   unavoidable, assumption as long as auxiliary information on vegetation volume fraction, as seen by a microwave
L-band radiometer, is not at hand. At the moment, no measurements for the vegetation volume fraction from L-band
radiometers exist according to the authors' knowledge. More details on the retrieval of the results shown in Figure
10 are provided in Meyer et al. (2019).
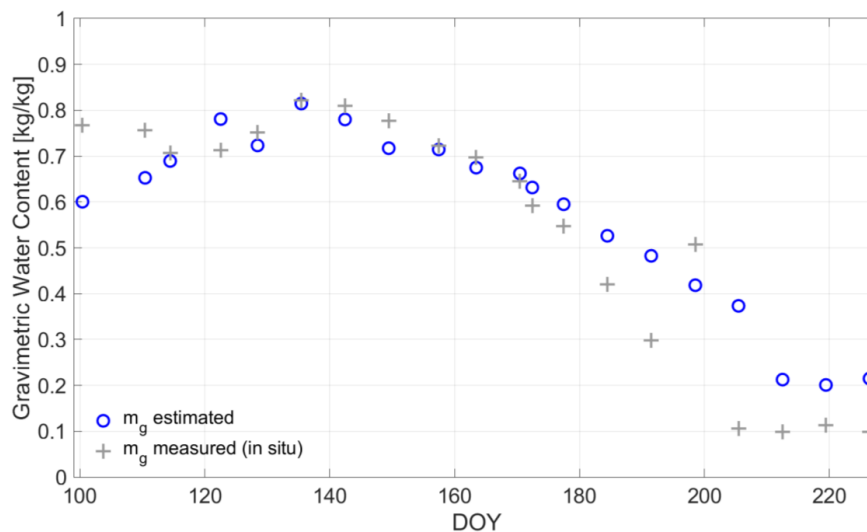
405   **Figure 10: Measured (gray crosses) and radiometer-derived (blue circles) gravimetric vegetation water content (m_g)**
[kg/kg] of winter wheat along days of year (DOY) in the growing season of 2017 at the field laboratory in Selhausen,
Germany (Meyer et al., 2019).

In Figure 11, the RWC_{Season} is shown for the entire growing period after calculus from (2) based on m_g. A
410   contrasting way of calculating RWC_{Season} [$\%$] from radiometer-based methods is reported in Rao et al. (2019), but
adopted by using the extremes of the VOD along growing season:

$$RWC_{Season,VOD} = \frac{VOD - VOD_{min}}{VOD_{max} - VOD_{min}} \cdot 100,$$ (8)

where VOD_{min} and VOD_{max} are the minimum and maximum of VOD within the recorded time series. By

calculating RWC_{Season} in this way, it is assumed that VOD is a direct indicator for m_g in wheat and does not

depend on biomass or vegetation structure. But, as can be seen from the course of $RWC_{Season,VOD}$ along growing

415   period (cf. Fig. 11), the water content is low for DOY 100 (tillering), since RWC-values are below 10 [-].

Afterwards, they increase until DOY 157 (onset of flowering with peak of vegetation height at DOY 149) to the

level of RWC_{Season}, calculated from (2). In this phase from tillering to flowering, also the main biomass and plant

structure developments of the wheat plants took place (cf. Fig. 1) and are also included in the VOD-signal. This

indicates one shortcoming of assessing the water content directly on basis of VOD, like in (8) (Fink et al., 2018;

420   Meyer et al., 2019). However, in periods of constant biomass, meaning times where only the water content in the

plants would change, RWC_{Season} could be directly estimated from VOD (Rao et al., 2019; Holtzman et al., 2020).
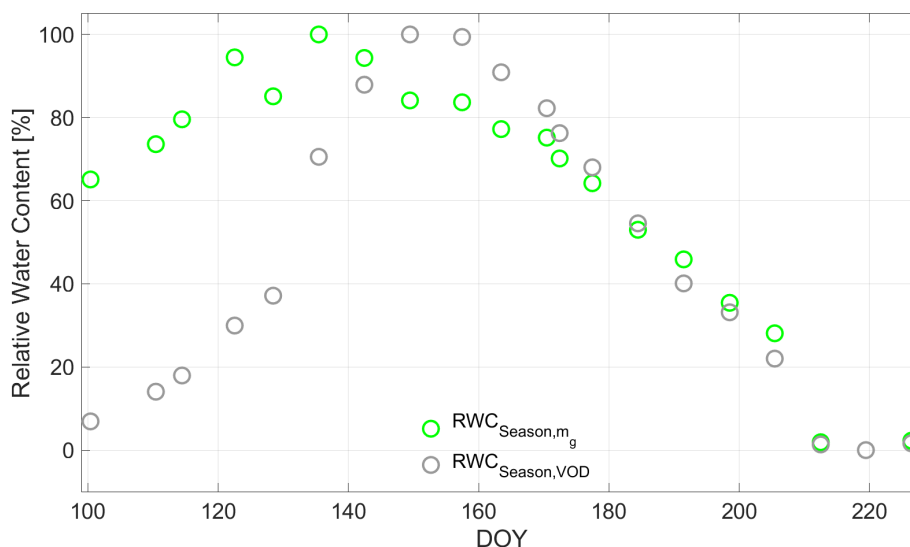
Figure 11: Seasonal Relative Water Content (RWC_{Season}) [%] calculated in (2) with radiometer-derived m_g (green circles) along growing season of 2017 in days of year (DOY) at the winter wheat field in Selhausen, Germany. The gray
425   **circles indicate RWC_{Season} calculated directly with the radiometer-derived vegetation optical depth (VOD) according to (9).**

From RWC_{Season}, the VWP of the winter wheat can be retrieved using (3) and assuming different change rates of

VWP according to RWC_{Season}-dynamics (cf. Fig. 3). Figure 12 shows in green color the intermediate change rate

430   and in a gray area between dashed curves the behavior of the VWP according to the differently assumed change

rates (blue color: slow change rate & red color: rapid change rate).

Hence, the influence of k_1 and k_2 in (3) is evident. The three different change rates (slow, intermediate and rapid) represent the possible spread of occurring RWC-VWP relationships for winter wheat and provide a potentially occurring VWP-value range resulting from the different change rate assumptions.

435   The common trends of the VWP-value range might be interpreted as guided by the precipitation inputs along the growing season (cf. Fig. 9): SMP in the top soil (0-5 [cm]), but also in the deeper soil layers (30 [cm]), increases to less negative values with each infiltrating precipitation impulse. Then, SMP gradually decreases in periods of dry downs (between the rain events, e.g. DOY 165 to DOY 175). VWP is not following SMP at any depth from DOY 100 to DOY 140 which might be partly due to the distinct phenological changes (stem elongation) and also caused

440   by the lower temperature regime, as mean daily temperature slowly increased from around 10 [$°C$] to about 20 [$°C$] in these 40 days (cf. Fig. 4). In addition, the vegetation water potential matches with SMP-values close to zero in this period (cf. Fig. 12). This indicates a sufficient water supply (close to or at field capacity) of the wheat plants with sufficient canopy hydration.
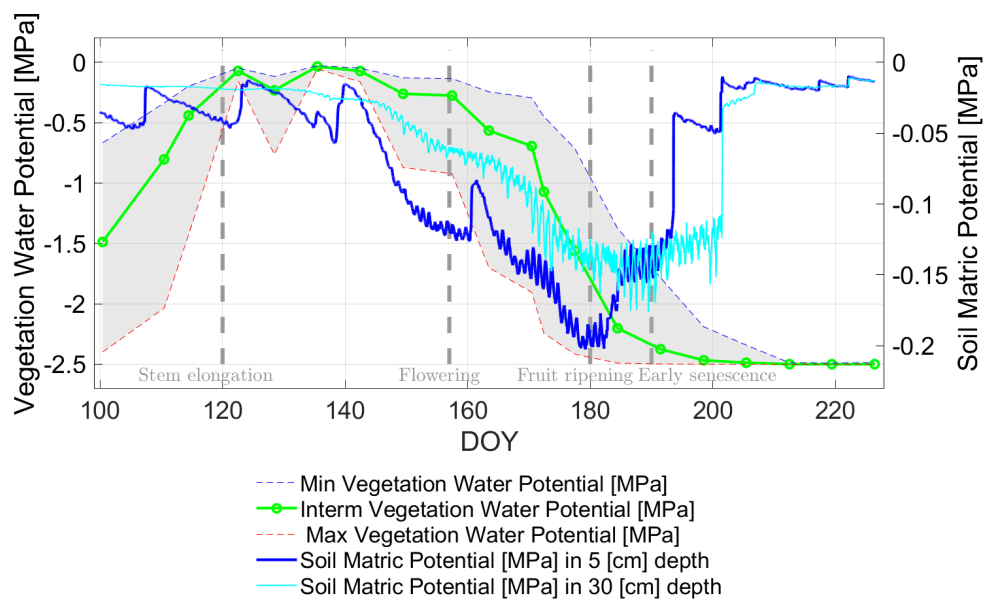
445

Figure 12: Comparison of in situ-based soil matric (both blueish curves) and radiometer-based vegetation water (green solid and small dashed curves) potentials (SMP [MPa] & VWP [MPa]) in the growing period of 2017 along days of year (DOY) at the winter wheat field. The gray-shaded area indicates the potential variability of the estimated VWP depending on applied relationship in (3) (cf. Fig. 3). Vertical dashed lines indicate major phenological phases of the

450   **winter wheat.**

A distinct decrease in VWP to more negative values occurs between DOY 140 and DOY 180. In line with results in Choudhury and Idso (1985), this decrease to strongly negative values is concurrent with a period of low rainfall and high evapotranspiration due to higher air temperature with a daily mean of around 20 [$°C$] (cf. Fig. 4) together

455 with maturing of the wheat in fruit development stage towards full biomass stage at DOY 191 (cf. also Tab. 1). For this, the different sampling rates for SMPs and VWP should be kept in mind, as SMPs and VWP origin from different sources (SMPs: in situ soil moisture measurements, VWP: L-band radiometer observations). However, the trend of both potentials (soil & vegetation) for the period of fully developed wheat canopy from DOY 140, with peak LAI at DOY 149 (cf. Fig. 4), to DOY 180 is apparently consistent and matching the in situ conditions of a

460 diminishing water availability in soil and subsequently for the wheat plants.

Due to the onset of senescence in the wheat stand (latest DOY 200), where water availability is not the limiting factor any more, the concurrency of SMPs and VWP trends along time vanishes completely. SMPs at both depths increase to less negative values by a series of irregular rain events starting from DOY 180 and VWP reaches the minimum of -2.5 [MPa] (cf. Fig. 12) at around DOY 200. This indicates that water loss in the plant due to senescence

465 processes (strong increase of R_{RX}) reached a stage where water content (m_g) falls to a minimum. Subsequently, VWP reaches its pre-defined minimum value (VWP_{min} = -2.5 [MPa]), which was set for the semi-empirical relationship between water content and water potential (cf. (3) and Fig. 3).

4.3. Seasonal Water Dynamics along the SPAS

Previous results (Figs. 10-12) presented the water filling status and the water potential in soil and wheat vegetation.

470 Now we want to take the results one step further by using the differences of the potentials (between atmosphere & vegetation as well as between vegetation & soil) together with soil, plant and atmosphere resistance estimates to assess water fluxes from soil to atmosphere: PWU and TR.

In Figure 13 the PWU [mm/s] (bluish curves) is depicted as time-variable uptake (depending on soil and root-xylem resistances used in (5)) together with its radiometer-based input parameter VWP (green curve). The other

475 input parameter in equation (5) is SMP which is illustrated in Figure 10 for both soil depths.

The blue PWU-curves in Figure 13 show on average a decline of water uptake until DOY 122. This results from a sufficient supply by precipitation water (SMP < -0.05 [MPa]) under low evaporative conditions (daily mean of VPD < 0.5 [kPa] & of air temperature around 10 [$°C$]) and wheat plants in tillering and early stem elongation phase,

but without major biomass development (DOY 122: LAI = 1.24 [-], plant height = 0.25 [m] & above ground

480   biomass = 0.24 [kg/m^2]; all values from Fig. 1 & Tab. 1).
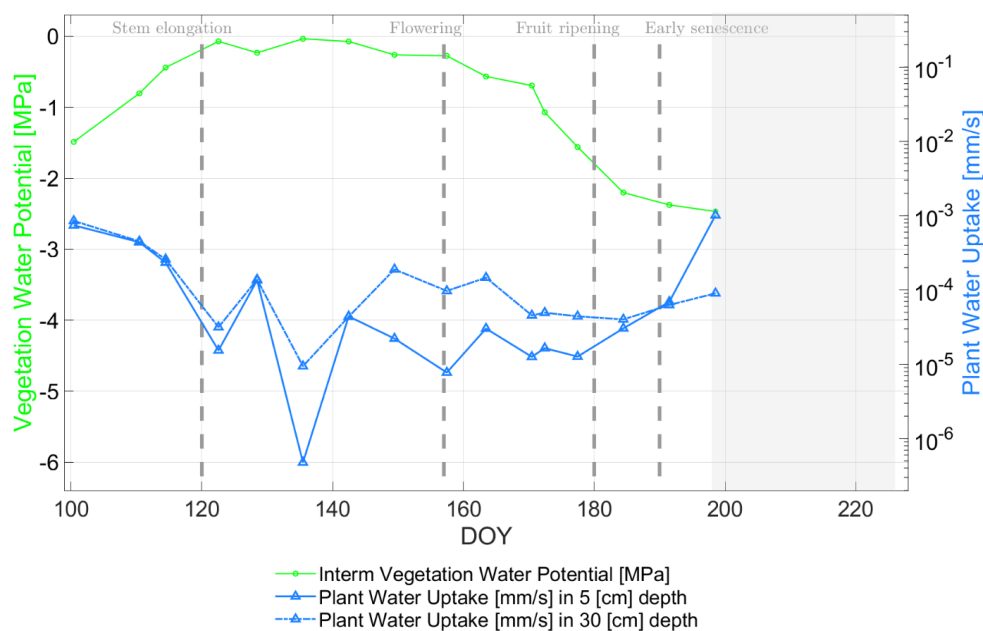
Figure 13: Comparison of radiometer-based plant water uptake PWU [mm/s] (blueish-colored curves with variable soil resistance at 5 [cm] and 30 [cm] soil depth) and vegetation water (green solid curve) potential VWP [MPa] along

485   **the growing season of 2017 for days of year (DOY) at the winter wheat field in Selhausen, Germany. The gray-masked area indicates the senescence phase where the water uptake estimates are not valid anymore due to simplifying assumptions in calculus of the root-xylem resistance. Vertical dashed lines indicate major phenological phases of the winter wheat.**

490   From DOY 122 to DOY 142 (stem elongation phase) the biomass level increased slightly, but due to the wheat stalk

development, the vegetation height and LAI changed significantly from 0.25 [m] to 0.56 [m] and 1.24 [-] to 3.6 [-],

respectively (cf. Fig. 1). Moreover, the soil hydraulic conductivity and the respective soil flow resistance R_S (cf.

Fig. 5) showed a steady decrease in water flow conditions at 30 [cm] depth and a fluctuating behavior due to rain

impulses at 5 [cm] depth. Hence, the PWU-curves (blueish lines in Fig. 13) show the same trends for 30 [cm] and

495   5 [cm] depth having a lower level of PWU at shallower soil depth resulting from smaller soil hydraulic conductivity

values (cf. Fig. 5). The root-xylem resistance R_{RX} in Figure 6 indicates a steady decrease until DOY 142, clearly

following its driving parameter LAI. The assumption behind is an increase in roots and xylem vessels concurrent to

leaf growth leading to an increase in flow capacities along plant development (Lynn and Carlson, 1990). Until DOY

142, PWU-curves are guided by R_{RX} rather than R_S due to stronger resistance values of the root-xylem system in

500 the early development stages of the winter wheat compared to a sufficiently watered soil for uptake (cf. Figs. 5 &
6).

Afterwards, PWU decreased and increased with different strength from DOY 142 until senescence phase (DOY >
190). First, there is a distinct decrease from DOY 142 to DOY 157 (inflorescence and flowering phase, cf. Tab. 1).
In this phase the soil moisture dropped mainly due to a daily mean air temperature of about 20 [$°C$] and absence of

505 major precipitation events, leading to a SMP-decrease from -0.03 [MPa] to -0.12 [MPa]. This is accompanied with
a significant increase in soil resistance (cf. Fig. 5) and a decrease in root-xylem resistance (cf. Fig. 6).

From DOY 157 to DOY 180 (flowering and grain development phase) rain input was absent and soil water decreased
with SMP–values up to -0.2 [MPa] on DOY 180 and a soil conductivity minimum of 1.1×10^{-13} [m/s] (cf.
Fig. 5). The VWP-values strongly dropped from -0.28 [MPa] to about -1.75 [MPa]. In this period PWU increased,

510 in the beginning stronger then only slightly, indicating water depletion from the soil (cf. Fig. 9) supporting in the
reproductive stage of the wheat plants.

In the last grain development phase (DOY 180 to DOY 190) before senescence (DOY > 190), the VWP further
decreased to -2.38 [MPa], but with a milder slope due to refilling water in soils (note that SMP for both soil depths
raised to -0.14 [MPa] during several consecutive rain events as seen in Figure 9 as gray bars). The PWU-curves at

515 5 [cm] depth start to rise again from DOY 191 to DOY 198 due to the first strong rain impulses seen first by the top
soil (cf. Fig. 13).

In the senescence phase (DOY 199), the soil moisture was not the limiting factor anymore and VWP dropped to
its pre-defined minimum of -2.5 [MPa] as soon as RWC reaches a level of 35 [$\%$], subsequently approaching almost
zero beyond DOY 210 (cf. Fig. 11). In Figure 11 a gray-masked area indicates the senescence phase where the

520 water uptake estimates are not valid anymore, since root-xylem resistance is considered to be solely dependent on
LAI in (6).

After uptake of water into the wheat plants, we focus in the following on water release from the wheat plants into
the atmosphere. In Figure 14, the estimated transpiration rates TR [mm/s] are shown along the growing season
including its input variables VWP and VPD. The general trend of the TR-curves indicate considerable

525 concurrency along season with the PWU-curves in Figure 13. Reviewing the principle of the SPAS, this connection
of dynamics, pointing towards steady water flow along the SPAS, supports the connection of the different water
storage compartments in the system.

However, their magnitudes are different especially around the ripening phase of the wheat (around DOY 180) due
to differently modelled time-variant flow resistances for both processes. This is more decisive for transpiration

530   (including radiation- and temperature-dependence within VPD) having a stronger diurnal cycle than water uptake

(including mainly moisture-dependence within soil matric potential). Hence the temporal dynamics and magnitudes

of TR and PWU exhibit no absolute concurrency due to dependence of TR to faster changing atmospheric

conditions, while dependence of PWU is on slower changing soil conditions.
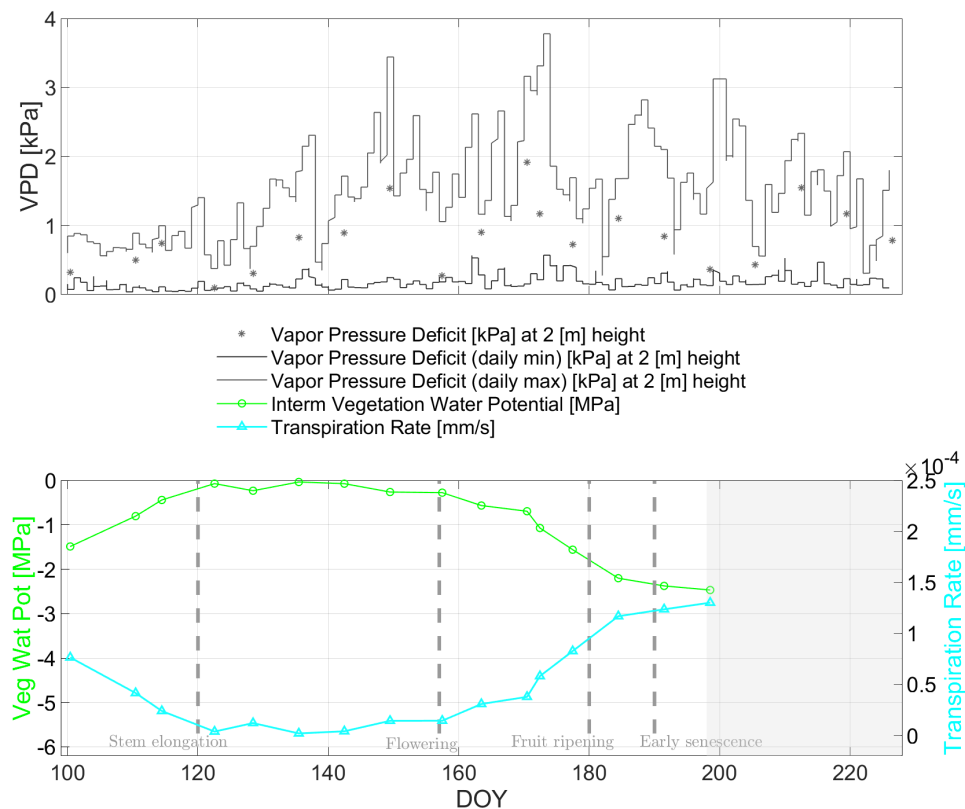
Figure 14: Top: Minimum and maximum of the vapor pressure deficit (VPD) [kPa] for atmospheric water need shown
535   **with gray lines. The asterisks indicate the VPD–values at time of radiometer measurement.**
Bottom: Comparison of radiometer-based transpiration rates TR [mm/s] (cyan curve for variable canopy &
aerodynamic resistances as well as a fixed cuticular resistance) and vegetation water (green curve) potential
VWP [MPa] along the growing period of 2017 for days of year (DOY) at the winter wheat field in Selhausen, Germany.
540   **The gray-masked area indicates the senescence phase where the assumption in the stomatal resistance calculus is not**
applicable. Vertical dashed lines indicate major phenological phases of the winter wheat.

Considering both flux estimates, the most interesting part is that for calculating PWU and TR two substantially

545   different in situ measurements (SMP, VPD) were paired together with the same radiometer-based VWP-input.

However, the dynamics of both fluxes (PWU, TR) are concurrent in trend and show considerable similarity along

wheat growing season. This comes with the caveat that the applied resistances of the soil-plant-atmosphere

compartments were derived from literature (R_C) or form auxiliary in situ information (e.g. soil hydraulic

conductivity, leaf area index, net solar radiation and wind speed) applied in empirical models (R_S, R_{RX}, R_{ST}, R_A),

550   (Manzoni et al., 2013b, Monteith & Unsworth, 2013). Nonetheless, VWP seems to be appropriate and fitting despite being a radiometer-based potential estimate between the on-site measurement-derived potentials of soil (SMP) and atmosphere (VPD).

5 Discussion

The presented study provides a radiometer-based approach to estimate time-dynamic flux rates (plant water uptake

555   & transpiration) from water status observations along the SPAS, even if assumptions on water flow properties (soil & plant hydraulic traits, e.g. effective soil porosity, rooting depth and flow resistances) and some ancillary data are necessary. With the proposed approach, analyses of the SPAS are enabled covering the different water pools (soil, plant and atmosphere), their potentials (suction tension) and in-between fluxes (uptake, transpiration). The estimates for each water pool are assessible together with a first analysis on how water flows from soil to the

560   atmosphere. It is encouraging that flux rates of PWU and TR (cf. Figs. 13 & 14) are overall concurrent and similar in trend despite different on-site information is included in the calculus of fluxes (PWU: Soil permittivity, TR: VPD). This might be a first indication to the feasibility to capture the continuous water flow within the SPAS by combining radiometer observations and in situ measurements.

In addition, the study relies on snapshot analysis of radiometer-based vegetation parameters (e.g. m_g, RWC and

565   VWP) for single days along the growing period, since radiometer measurements were only conducted over one to two hours within 9 am and 2 pm on a measuring day. No analyses about the diurnal cycle of RWC, VWP, PWU and TR or their sub-daily variability within the wheat canopy can be provided. Thus, all results are representative with respect to their trends along the growing season.

The presented results indicate the unique potential of using passive microwave observations with on-site

570   information of soil and atmosphere to estimate seasonal water dynamics for a single winter wheat field. As the setup of the experiment at the Selhausen field laboratory is temporally confined (one growing season), specific in setup (metal mesh for soil signal blockage; only vegetation-related signals included), small-scale (one field) and single-species (only winter wheat), it is at this moment not possible to significantly generalize the presented results with respect to other temporal, spatial or species domains and scales. Especially, generalizing the method is

575   challenging as, for instance, the RWC to VWP conversion (cf. Fig. 3) is plant type-specific and not yet well understood for spatio-temporal resolution conditions of satellite radiometer (passive microwave) remote sensing with resolutions of kilometers in space and days in time (cf. Fig. 2 in Konings et al., 2019). In detail, the conversion

from RWC to VWP is semi-empirical. This means the rate and strength of water supply on potential (suction)

reduction is not accessible at field scale and along growing season from the on-site measurements, but in a first

580   attempt deducible from literature survey (Turner and Long, 1980; Turner, 1988; Zweifel and Häsler, 2000; Zweifel

et al., 2001; Pearcy et al., 2012).

As mentioned above, there are some limitations of the retrieval to arrive from water status at water fluxes. Since

effective variables, like the soil, wheat canopy and atmospheric resistances, cannot be directly measured in situ at

the field scale, they are estimated by (wheat-specific) mechanistic retrieval models for soil, root-xylem, stomatal

585   and aerodynamic resistances fed with (auxiliary) on-site measurements (cf. sections 3.2 & 3.4 for details).

However, the mechanistic models are empirically derived and therefore not complete in terms of all potentially

occurring flow resistances within the wheat plants, e.g. intercellular air space resistance. For simplicity the same

transpiration from top (adaxial) and bottom (abaxial) side of leaf is assumed (cf. (7) & cf. Nobel, 2020, p.415 and

427ff).

590   Another fundamental specificity of the study setup, mentioned briefly above, is that the soil emission is completely

blocked physically by a metal mesh on the ground (ideal investigation conditions for vegetation influence on

microwave emission and scattering). This could represent a burden on wide-area monitoring of water dynamics

with radiometer-based retrievals. However, a joint approach combining emission modeling and data inversion (e.g.

using zeroth- or first-order radiative transfer models (Wigneron et al., 2017)) was used in Meyer et al. (2018) on

595   another part of the wheat field without mesh coverage. Soil and vegetation emission signals were separated leading

to equivalent estimates of soil moisture and VOD compared to the values from the mesh-covered part (VOD) and

from the in situ measurements (soil moisture). Hence, this might pave the way towards a wide-area retrieval of

water dynamics with radiometers, here at L-band. Algorithms from operating satellite radiometer missions would

be available, such as from SMAP (Konings et al., 2017).

600   Despite all restrictions (due to having no complete measurement portfolio of all SPAS variables), rather no attempts

are reported in literature trying a similar kind of approach combining soil, plant and atmosphere information from

L-band passive radiometry with (on-site) measurements at the field scale. One exception is the correlation of L-

band radiometer-derived VOD with water potential measurements of a tree stand at Harvard forest along one

growing season (Holtzman et al., 2020). In any case, there is a need of remote sensing-scale analyses of transfer-

605   functions from VOD via water content to water potential in plants, which must be different from laboratory

analyses of single tissues of leaves (Turner, 1988).
In the end, this is a path finder study to water dynamics across winter wheat starting from ground-based L-band radiometry in combination with on-site measurements of soil and atmosphere. Our results show the potential of combining microwave radiometer-based estimates with in situ measurements into crop growth or soil-plant-atmosphere transport models, in agreement with previous studies (Wang and Engel, 2002; Palosuo et al., 2011). Furthermore, atmosphere and soil information, like the VPD or soil moisture, can also be derived today from remote sensing sources, e.g. VPD from Atmospheric Infrared Sounder (AIRS) on-board NASA's Aqua satellite (Feldman et al., 2020) or surface soil moisture from SMAP or SMOS microwave radiometer missions (Entekhabi et al., 2010; Kerr et al., 2010). In addition, all soil-plant-atmosphere parameters, needed as input in the presented water dynamic calculus and listed in Table 2, can already be estimated today from multi-sensor remote sensing, including lidars (vegetation height), optical sensors (solar net radiation, VPD, LAI), radars/scatterometers (wind speed, vegetation volume fraction, soil moisture, VOD) and radiometers (VOD, soil moisture, wind speed). In this way, the study sheds light on a future assessment of the SPAS, solely relying on a combination of multi-sensor remote sensing, preferably on satellite basis. This would enable a wide-area (up to global) assessment of the SPAS in the end.

Hence, direct implication of this field-based study is that with more measurements or wider knowledge about plant characteristics regarding water flux, the approach should be applicable to more plant types and to larger areas exploiting the wide-area mapping capabilities of space-borne sensors. Future missions, like the Copernicus Imaging Microwave Radiometer (CIMR) of the European Space Agency (ESA) (Kilic et al., 2018), could be potential candidates to address research on water fluxes within the SPAS on global scale exploiting the benefit of having multiple sensing frequencies allowing for different penetration and transmission capabilities through vegetation canopies (Prigent and Jiménez, 2021; Zhao et al., 2021). Advanced methodologies exploiting the synergies from present and planned satellite constellations will possibly allow a frequent and large-scale mapping of water fluxes through the SPAS.

6 Conclusions

The objective of this study was to investigate whether observations of a ground-based radiometer over a winter wheat field allow to estimate seasonal flux rates of water (plant water uptake and transpiration) along the soil-plant-atmosphere system (SPAS). We started from L-band radiometry-based vegetation optical depth (VOD)

flanked by on-site measurements of soil and atmosphere. The major research question behind the objective was

635   how far L-band radiometry and on-site measurements contain enough information to derive water potentials and

flux rates in the SPAS of the winter wheat field along the growing season.

From the presented study, first conclusions can be drawn within the boundaries of the experimental setup, detailed

in the former sections. Arriving at exact water fluxes in the SPAS of winter wheat needs further information (e.g.

about soil, plant and atmosphere resistances) than initially made during the presented campaign in 2017 at the

640   Selhausen (Germany) field laboratory. The campaign was originally not designed for studying water fluxes in the

SPAS. Existing on-site measurements of soil (permittivity), plant (height & LAI) and atmosphere (net radiation,

temperature & relative humidity of air) were used in the study to estimate water flux rates (PWU & TR). Hence,

it is imperative to have water status information (θ, m_g, RH) along the SPAS for estimating water dynamics (cf.

Fig. 2). Otherwise these dynamics cannot be fully assessed. Furthermore, soil moisture is required from in situ

645   measurements or estimated from radiometer observations. In this work we used in situ measurements, which had

a higher temporal resolution.

Our study shows possible ways to incorporate L-band radiometry (ground-based remote sensing) in a field-based

SPAS assessment. We were able to obtain reasonable estimates of water potentials and water flux rates in the SPAS

in terms of the major trend along season. The presented results reveal the capacity of L-band radiometers in

650   combination with in situ measurements to assess water dynamics within the SPAS of a wheat field. However, the

estimation of absolute accuracies needs to be tackled in future studies with available in situ measurements of water

dynamics (potentials & flux rates).

This work sheds light into the potential of radiometer-integrated SPAS research. Our proposed approach should be

further explored with dedicated field laboratory studies, explicitly including ground-based (L-band) radiometry

655   and other remote sensing sensors together with in situ measurements (still) necessary to validate water flux

dynamics, such as soil water potential, leaf water potential, sap flux, stomatal conductance and transpiration rates.

We advocate in the future, a fully remote sensing-based, wide-area (up to global) SPAS assessment can be a major

achievement following the initial results of this study.

660   *Acknowledgments.* The authors thank Mr. Andrew Feldman (MIT), Prof. Dr. Dara Entekhabi (MIT), Dr. Stan Schymanski
(LIST) and Prof. Dr. Jordi Martínez-Vilalta (CREAF) for their helpful comments and suggestions supporting this research. The
authors want to acknowledge MIT for supporting this research with the MIT-Germany Seed Fund "Global Water Cycle and
Environmental Monitoring using Active and Passive Satellite-based Microwave Instruments" and with the MIT-Belgium UCL
Seed Fund "Early Detection of Plant Water Stress Using Remote Sensing". The ELBARA-II radiometer was provided by the

665   Terrestrial Environmental Observatories (TERENO) initiative funded by the Helmholtz Association of German Research
Centers. D.C. has received funding by "la Caixa" Foundation (ID 100010434), under agreement LCF/PR/MIT19/51840001, by
the MIT-MISTI, and by the Spanish government through projects ESP2017-89463-C3-2-R and MDM-2016-0600.

Author Contributions. Conceptualization, T.J., F.J. and M.P.; Methodology, T.J., A.F., F.J., D.C. and M.P.; Software, T.J., F.J.,
670   A.F. and T.M.; Formal Analysis, All; Data Curation, T.M., F.J., T.J. and A.F.; Writing-Original Draft Preparation, T.J., A.F.,
F.J., D.C., M.J.B. and M.P.; Writing-Review & Editing, All; Visualization, T.J., A.F., F.J., M.J.B. and T.M.; Supervision, M.P..

Data availability. All data were recorded by Forschungszentrum Jülich, Institute of Bio- and Geosciences, Agrosphere (IGB-
3), and are partly available upon request from François Jonard (f.jonard@fz-Juelich.de). TERENO data are available at
675   www.tereno.net.

Competing interests.The authors declare that they have no conflict of interest.

References

680   Alduchov, O. A., and Eskridge, R. E.: Improved Magnus form approximation of saturation vapor pressure, Journal
of applied meteorology, 35(4), 601-609, 1996.

Allen, R. G., Pereira, L. S., Raes, D., and Smith, M.: Crop evapotranspiration-Guidelines for computing crop water
requirements-FAO Irrigation and drainage paper 56, FAO, Rome, 300(9), D05109, 1998.

Blizzard, W.E. and Boyer, J.S.: Comparative resistance of the soil and the plant to water transport. Plant
685   physiology, 66(5), 809-814, 1980.

Bonan, G. B., Williams, M., Fisher, R. A., and Oleson, K. W.: Modeling stomatal conductance in the earth system:
linking leaf water-use efficiency and water transport along the soil–plant–atmosphere continuum. Geoscientific
Model Development, 7(5), 2193-2222, 2014.

Brooks, R.H. and Corey, A.T., Properties of porous media affecting fluid flow, in J. Irrig. Drain. Div. 92, 61–90,
690   1964.

Campbell, G.: A simple method for determining unsaturated conductivity from moisture retention data, in Soil
Sci., 117, 311-314, 1974.

Castellvi, F., Perez, P.J., Villar, J.M. and Rosell, J.I.: Analysis of methods for estimating vapor pressure deficits
and relative humidity, Agricultural and Forest Meteorology, 82(1-4), 29-45, 1996.

695   Choat, B., Brodribb, T. J., Brodersen, C. R., Duursma, R. A., López, R., and Medlyn, B. E.: Triggers of tree
mortality under drought, Nature, 558(7711), 531-539, 2018.

Choudhury, B.J. and Idso, S.B.: An empirical model for stomatal resistance of field-grown wheat, Agricultural and
forest meteorology, 36(1), 65-82, 1985.

Choudhury, B. J., and Idso, S. B.: Evaluating plant and canopy resistances of field-grown wheat from concurrent
700   diurnal observations of leaf water potential, stomatal resistance, canopy temperature, and evapotranspiration flux,
Agricultural and forest meteorology, 34(1), 67-76, 1985.

Clapp, R.B. and Hornberger, G.M.: Empirical equations for some soil hydraulic properties, in Water Resour. Res.
14, 601–604, 1978.

Cowan, I. R.: Transport of water in the soil-plant-atmosphere system, Journal of Applied Ecology, 221-239, 1965.

705   Damour, G., Simonneau, T., Cochard, H., and Urban, L.: An overview of models of stomatal conductance at the
leaf level, Plant, Cell and Environment, 33(9), 1419-1438, 2010.

Dingman, S. L.: Physical hydrology. Waveland Press, Long Grove, USA, 2015.

Duursma, R. A., Blackman, C. J., Lopéz, R., Martin-StPaul, N. K., Cochard, H., and Medlyn, B. E.: On the
minimum leaf conductance: its role in models of plant water use, and ecological and environmental controls, New
710   Phytologist, 221(2), 693-705, 2019.

Eamus, D., Huete, A., and Yu, Q.: Vegetation dynamics, Cambridge University Press, U.K., 2016.

Elfving, D.C., Kaufmann, M.R., and Hall, A.E.: Interpreting leaf water potential measurements with a model of
the soil-plant-atmosphere continuum, Physiologia plantarum, 27(2), 161-168, 1972.

Entekhabi, D., Njoku, E. G., O'Neill, P. E., Kellogg, K. H., Crow, W. T., Edelstein, W. N., et al.: The soil moisture
715   active passive (SMAP) mission, Proceedings of the IEEE, 98(5), 704-716, 2010.

Fan, J., McConkey, B., Wang, H., and Janzen, H.: Root distribution by depth for temperate agricultural crops, Field
Crops Research, 189, 68-74, 2016.

Feddes, R. A., and Rijtema, P. E.: Water withdrawal by plant roots, Journal of Hydrology, 17(1-2), 33-59, 1972.

Feldman, A.F., Short Gianotti, D.J., Trigo, I.F., Salvucci, G.D. and Entekhabi, D.: Land-atmosphere drivers of
720   landscape-scale plant water content loss, Geophysical Research Letters: Hydrology and Land Surface Studies,
DOI: 10.1029/2020GL090331, 2021.

Fink, A., Jagdhuber, T., Piles, M., Grant, J., Baur, M., Link, M., and Entekhabi, D.: Estimating Gravimetric
Moisture of Vegetation Using an Attenuation-Based Multi-Sensor Approach, In IGARSS 2018-2018 IEEE
International Geoscience and Remote Sensing Symposium (353-356). IEEE, 2018.

725   Frank, A. B., Power, J.F., and Willis, W.O.: Effect of Temperature and Plant Water Stress on Photosynthesis,
Diffusion Resistance, and Leaf Water Potential in Spring Wheat, Agronomy journal, 65(5), 777-780, 1973.

Gallardo, M., Eastham, J., Gregory, P.J. and Turner, N.C.: A comparison of plant hydraulic conductances in wheat
and lupins, Journal of Experimental Botany, 47(2), 233-239, 1996.

Gardner, W. R.: Dynamic aspects of water availability to plants, Soil science, 89(2), 63-73, 1960.

730   Gardner, W. R.: Dynamic aspects of soil-water availability to plants, Annual review of plant physiology, 16(1), 323-342, 1965.

Gupta, A. S., Berkowitz, G. A., and Pier, P. A.: Maintenance of photosynthesis at low leaf water potential in wheat: role of potassium status and irrigation history, Plant Physiology, 89(4), 1358-1365, 1989.

Gupta, S.C. and Wang, D.: Water Retention in Soil, in Encyclopedia of Soil Science, R. Lal (Ed.), CRC Press,
735   Taylor and Francis Group, Boca Raton, FL, USA, ISBN: 9780849350542, 2006.

Hillel, D. Fundamentals of soil physics, Academic Press. New York, 1980.

Holtzman, N., Anderegg, L.D.L., Kraatz, S., Mavrovic, A., Sonnentag, O., Pappas, C., Cosh, M.H., Langlois, A., Lakhankar, T., Tesser, D., Steiner, N., Colliander, A., Roy, A., and Konings, A.G.: L-band vegetation optical depth as an indicator of plant water potential in a temperate deciduous forest stand, Biogeosciences, 18, 739-753, 2021.

740   Johnson, K. M., Jordan, G. J., and Brodribb, T. J.: Wheat leaves embolized by water stress do not recover function upon rewatering, Plant, Cell and Environment, 41(11), 2704-2714, 2018.

Jonard, F., Weihermüller, L., Schwank, M., Jadoon, K. Z., Vereecken, H., and Lambot, S.: Estimation of hydraulic properties of a sandy soil using ground-based active and passive microwave remote sensing, IEEE transactions on geoscience and remote sensing, 53(6), 3095-3109, 2015.

745   Jonard, F., Bircher, S., Demontoux, F., Weihermüller, L., Razafindratsima, S., Wigneron, J. P., and Vereecken H.: Passive L-band microwave remote sensing of organic soil surface layers: a tower-based experiment, Remote Sensing, 10(2): 304, 2018.

Jonard F., De Cannière S., Brüggemann N., Gentine P., Short Gianotti D. J., Lobet G., Miralles D. J., Montzka C., Pagán B. R., Rascher U., and Vereecken H.: Value of chlorophyll fluorescence for quantifying hydrological states
750   and fluxes: Current status and challenges, Agricultural and Forest Meteorology, 291: 108088. https://doi.org/10.1016/j.agrformet.2020.108088, 2020.

Kameli, A., and Lösel, D. M.: Carbohydrates and water status in wheat plants under water stress, New Phytologist, 125(3), 609-614, 1993.

Kerr, Y. H., Waldteufel, P., Wigneron, J. P., Delwart, S., Cabot, F., Boutin, J., et al.: The SMOS mission: New
755   tool for monitoring key elements of the global water cycle, Proceedings of the IEEE, 98(5), 666-687, 2010.

Kilic, L., et al.: Expected performances of the Copernicus Imaging Microwave Radiometer (CIMR) for an all-weather and high spatial resolution estimation of ocean and sea ice parameters, Journal of Geophysical Research: Oceans 123.10, 7564-7580, 2018.

Konings, A. G., Piles, M., Das, N., and Entekhabi, D.: L-band vegetation optical depth and effective scattering
760   albedo estimation from SMAP, Remote Sensing of Environment, 198, 460-470, 2017.

Konings, A. G., Rao, K., and Steele-Dunne, S. C.: Macro to micro: microwave remote sensing of plant water content for physiology and ecology, New Phytologist, 223(3), 1166-1172, 2019.

Lambers, H., Stuart Chapin III, F., and Pons T.L.: Plant physiological ecology, Springer Science and Business Media, 2008.

765   Lynn, B. H., and Carlson, T. N.: A stomatal resistance model illustrating plant vs. external control of transpiration, Agricultural and Forest Meteorology, 52(1-2), 5-43, 1990.

Manzoni, S., Vico, G., Porporato, A., and Katul, G.: Biological constraints on water transport in the soil–plant–atmosphere system, Advances in Water Resources, 51, 292-304, 2013a.

Manzoni, S., Vico, G., Katul, G., Palmroth, S., Jackson, R. B., and Porporato, A.: Hydraulic limits on maximum
770   plant transpiration and the emergence of the safety–efficiency trade-off, New Phytologist, 198(1), 169-178, 2013b.

Manzoni, S., Vico, G., Katul, G., Palmroth, S., and Porporato, A.: Optimal plant water-use strategies under stochastic rainfall, Water Resources Research, 50(7), 5379-5394, 2014.

Margulis, S. A.: Introduction to hydrology, https://ucla.app.box.com/v/Intro-to-Hydrology-pdf, 2017.

Martínez-Vilalta, J., and Garcia-Forner, N.: Water potential regulation, stomatal behaviour and hydraulic transport
775   under drought: deconstructing the iso/anisohydric concept, Plant, Cell and Environment, 40(6), 962-976, 2017.

Martinez-Vilalta, J., Anderegg, W. R., Sapes, G., and Sala, A.: Greater focus on water pools may improve our ability to understand and anticipate drought-induced mortality in plants, New Phytologist, 2019.

Matheny, A. M., Mirfenderesgi, G., and Bohrer, G.: Trait-based representation of hydrological functional properties of plants in weather and ecosystem models, Plant diversity, 39(1), 1-12, 2017.

780   Meyer, T., Weihermüller, L., Vereecken, H., and Jonard, F.: Vegetation Optical Depth and Soil Moisture Retrieved from L-Band Radiometry over the Growth Cycle of a Winter Wheat, Remote Sensing, 10(10), 1637, 2018.

Meyer, T., Jagdhuber, T., Piles, M., Fink, A., Grant, J., Vereecken, H., and Jonard, F.: Estimating Gravimetric Water Content of a Winter Wheat Field from L-Band Vegetation Optical Depth. Remote Sensing, Remote Sensing 11(20), 2353, 2019.

785   Momen, M., and Bou-Zeid, E.: Analytical reduced models for non-stationary diabatic atmospheric boundary layers, Boundary-Layer Meteorology, 164(3), 383–399. https://doi.org/10.1007/s10546-017-0247-0, 2017.

Momen, M., Wood, J. D., Novick, K. A., Pangle, R., Pockman, W. T., McDowell, N. G., and Konings, A. G.: Interacting effects of leaf water potential and biomass on vegetation optical depth, Journal of Geophysical Research: Biogeosciences, 122(11), 3031-3046, 2017.

790   Monteith, J. L.: Evaporation and environment. In Symposia of the society for experimental biology, 19, 205-234. Cambridge University Press (CUP) Cambridge, 1965.

Monteith, J., and Unsworth, M.: Principles of environmental physics: plants, animals, and the atmosphere. Academic Press. Cambridge, USA, 2013.

Nobel, P.S.: Physicochemical and Environmental Plant Physiology, Academic Press. Cambridge, USA, 2020.

795 Oosterhuis, D. M., and Walker, S.: Stomatal resistance measurement as an indicator of water deficit stress in wheat and soybeans, South African Journal of Plant and Soil, 4(3), 113-120, 1987.

Palosuo, T., Kersebaum, K. C., Angulo, C., Hlavinka, P., Moriondo, M., Olesen, J. E., et al.: Simulation of winter wheat yield and its variability in different climates of Europe: a comparison of eight crop growth models, European Journal of Agronomy, 35(3), 103-114, 2011.

800 Passioura, J. B.: Water in the soil-plant-atmosphere continuum, In Physiological plant ecology II (5-33). Springer, Berlin, Heidelberg, 1982.

Pearcy, R. W., Ehleringer, J. R., Mooney, H., and Rundel, P. W. (Eds.). Plant physiological ecology: field methods and instrumentation, Springer Science and Business Media, 2012.

Portal, G., Jagdhuber, T., Vall-llossera, M., Camps, A., Pablos, M., Entekhabi, D., and Piles, M.: Assessment of
805 Multi-Scale SMOS and SMAP Soil Moisture Products across the Iberian Peninsula, Remote Sensing, 12(3), 570, 2020.

Prigent, C., and Jimenez, C.: An evaluation of the synergy of satellite passive microwave observations between 1.4 and 36 GHz, for vegetation characterization over the Tropics, Remote Sensing of Environment, 257, 112346, 2021.

810 Rao, K., Anderegg, W. R., Sala, A., Martínez-Vilalta, J., and Konings, A. G.: Satellite-based vegetation optical depth as an indicator of drought-driven tree mortality, Remote Sensing of Environment, 227, 125-136, 2019.

Rascio, A., Platani, C., Scalfati, G., Tonti, A., and Di Fonzo, N.: The accumulation of solutes and water binding strength in durum wheat, Physiologia Plantarum, 90(4), 715-721, 1994.

Reichardt, K., and Timm, L. C.: Soil, plant and atmosphere, Springer Nature Switzerland, Cham, Switzerland,
815 2014.

Ritchie, J. T.: Water dynamics in the soil-plant-atmosphere system, Plant and Soil, 81-96, 1981.

Ruggiero, C., Angelino, G., Maggio, A.: Developmental regulation of water uptake in wheat, Journal of Plant Physiology, 164, 1170-1178, 2007.

Sadeghi, M., Gao, L., Ebtehaj, A., Wigneron, J. P., Crow, W. T., Reager, J. T., and Warrick, A. W.: Retrieving
820 global surface soil moisture from GRACE satellite gravity data, Journal of Hydrology, 584, 124717, 2020a.

Sadeghi, M., et al.: Global estimates of land surface water fluxes from SMOS and SMAP satellite soil moisture data, Journal of Hydrometeorology 21.2, 241-253, 2020b.

Schmugge, T.J and; Jackson, T.J.: A dielectric model of the vegetation effects on the microwave emission from soils, IEEE Trans. Geosci. Remote Sens., 30, 757–760, 1992.

825   Shukla, M.K.: Soil physics. An Introduction, CRC Press, Taylor and Francis Group, Boca Raton, FL, USA, ISBN: 9781439888421, 2014.

Siddique, M. R. B., Hamid, A. I. M. S., and Islam, M. S.: Drought stress effects on water relations of wheat, Bot. Bull. Acad. Sin, 41(1), 35-39, 2000.

Slatyer, R. O., and Taylor, S. A.: Terminology in plant-and soil-water relations, Nature, 187(4741), 922-924, 1960.

830   Smart, R. E., and Bingham, G. E.: Rapid estimates of relative water content, Plant physiology, 53(2), 258-260, 1974.

Steenpass, C., Vanderborght, J., Herbst, M., Šimůnek, J., and Vereecken, H.: Estimating soil hydraulic properties from infrared measurements of soil surface temperatures and TDR data, Vadose zone journal, 9(4), 910-924, 2010.

Topp, G.C., Davis, J.L. and Annan, A.P.: Electromagnetic determination of soil water content: measurements in
835   coaxial transmission lines, in Water Resources Research, 1 6(3), 574-582, DOI: 10.1029/WR016i003p00574, 1980.

Turner, N. C., and Long, M. J.: Errors arising from rapid water loss in the measurement of leaf water potential by the pressure chamber technique, Functional Plant Biology, 7(5), 527-537, 1980.

Turner, N. C.: Measurement of plant water status by the pressure chamber technique, Irrigation science, 9(4), 289-
840   308, 1988.

Tyree, M. T., and Zimmermann, M. H.: Xylem structure and the ascent of sap, Springer Science and Business Media, 2013.

Ulaby, F. and El-Rayes, M.: Microwave dielectric spectrum of vegetation—Part II: Dual-dispersion model, IEEE Trans. Geosci. Remote Sens., 5, 550–557, 1987.

845   Van den Honert, T. H.: Water transport in plants as a catenary process, Discussions of the Faraday Society, 3, 146-153, 1948.

van Genuchten, M.T.: A Closed-form Equation for Predicting the Hydraulic Conductivity of Unsaturated Soils, in Soil Science Society of America Journal, 44, 892-898, DOI:10.2136/sssaj1980.03615995004400050002x, 1980.

Wallace, J. S.: Water transport and leaf water relations in winter wheat crops, Doctoral dissertation, University of
850   Nottingham, 1978.

Wallace, J. S., and Biscoe, P. V.: Water relations of winter wheat: 4. Hydraulic resistance and capacitance in the soil-plant system, The Journal of Agricultural Science, 100(3), 591-600, 1983.

Wang, E., and Engel, T.: Simulation of growth, water and nitrogen uptake of a wheat crop using the SPASS model, Environmental Modelling and Software, 17(4), 387-402, 2002.

855   Ward, R. C., and Robinson, M. Principles of hydrology, 3rd edition. McGraw-Hill, London, 2014.

Wigneron, J-P., et al.: Modelling the passive microwave signature from land surfaces: A review of recent results and application to the L-band SMOS and SMAP soil moisture retrieval algorithms, Remote Sensing of Environment, 192, 238-262, 2017.

Yang, S. J., and Jong, E. D.: Effect of soil water potential and bulk density on water uptake patterns and resistance
860   to flow of water in wheat plants, Canadian Journal of Soil Science, 51(2), 211-220, 1971.

Zhao, T., Shi, J., Entekhabi, D., Jackson, T. J., Hu, L., Peng, Z., et al.: Retrievals of soil moisture and vegetation optical depth using a multi-channel collaborative algorithm, Remote Sensing of Environment, 257, 112321, 2021.

Zweifel, R. and Häsler, R.: Stem radius changes and their relation to stored water in stems of young Norway spruce trees, Trees, 15(1), 50-57, 2000.

865   Zweifel, R., Item, H., and Häsler, R.: Link between diurnal stem radius changes and tree water relations, Tree physiology, 21(12-13), 869-877, 2001.